The new nitrogen dioxide (NO2) linelist in the GEISA database and first identification of the $\nu 1+2\nu 3$-$\nu 3$ band of 14N16O2

Agnès Perrin, L. Manceron, J.-M. Flaud, F. Kwabia-Tchana, Raymond Armante, P. Roy, D. Doizi

Journal Pre-proofs

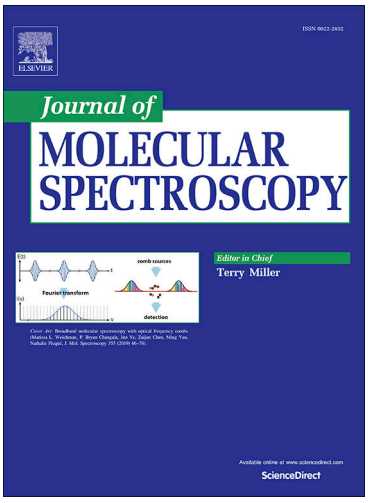

The new nitrogen dioxide (NO_2) linelist in the GEISA database and first identification of the $\nu_1+2\nu_3-\nu_3$ band of $^{14}N^{16}O_2$

Agnès Perrin, L. Manceron, J.-M. Flaud, F. Kwabia-Tchana, R. Armante, P. Roy, D. Doizi

PII: S0022-2852(20)30162-4
DOI: https://doi.org/10.1016/j.jms.2020.111394
Reference: YJMSP 111394

To appear in: *Journal of Molecular Spectroscopy*

Received Date: 21 September 2020
Revised Date: 30 October 2020
Accepted Date: 21 November 2020

Please cite this article as: A. Perrin, L. Manceron, J.-M. Flaud, F. Kwabia-Tchana, R. Armante, P. Roy, D. Doizi, The new nitrogen dioxide (NO_2) linelist in the GEISA database and first identification of the $\nu_1+2\nu_3-\nu_3$ band of $^{14}N^{16}O_2$, *Journal of Molecular Spectroscopy* (2020), doi: https://doi.org/10.1016/j.jms.2020.111394

The new nitrogen dioxide (NO_2) linelist in the GEISA database; first identification of the $\nu_1+2\nu_3-\nu_3$ band of $^{14}N^{16}O_2$.

Agnès Perrin[a,*]
L. Manceron [b,c],
J.-M. Flaud[d],
F. Kwabia-Tchana [d],
R. Armante [a]
P.Roy[b]
D. Doizi [e]

[a]Laboratoire de Météorologie Dynamique/IPSL, UMR CNRS 8539, Ecole Polytechnique, Université Paris-Saclay, RD36, 91128 Palaiseau Cedex, France
.[b] Ligne AILES, Synchrotron SOLEIL, L'Orme des Merisiers, St-Aubin BP48, 91192 Gif-sur-Yvette Cedex, France.
[c] Sorbonne Université, CNRS, MONARIS, UMR 8233, 4 place Jussieu, Paris, F-75005 France

[d] Laboratoire Interuniversitaire des Systèmes Atmosphériques (LISA), UMR CNRS 7583, Université de Paris et Université Paris Est Créteil, Institut Pierre Simon Laplace (IPSL), 61 Avenue du Général de Gaulle, F-94010 Créteil Cedex, France
[e] Université Paris-Saclay, CEA, Service d'Etude du Comportement des Radionucléides, 91191, Gif-sur-Yvette, France

Number of tables: 5
Number of figures: 11

* Corresponding author: agnes.perrin@lmd.ipsl.fr,

Keywords: Nitrogen dioxide; $^{14}N^{16}O_2$; Fourier transform spectroscopy; Electron spin-rotation resonances; Vibration-rotation resonances; HITRAN; GEISA;

Abstract

We have generated new lists of line position, line intensity and line shape parameters of nitrogen dioxide ($^{14}N^{16}O_2$ and $^{15}N^{16}O_2$), here labeled as "GEISA-19", which have been included in the (Gestion et Etude des Informations Spectroscopiques Atmosphériques) GEISA database (https://geisa.aeris-data.fr/). Except for the far infrared and the 13.3 μm regions, all spectral regions of the 1153- 4775 cm^{-1} spectral domain are significantly modified by this major update of the GEISA linelist. For the 6.2 μm and 3.4 μm spectral regions, which correspond to the strongest absorption of NO_2, we proceed to a complete replacement of the lists for the first hot bands, $\nu_2+\nu_3-\nu_2$ and $\nu_1+\nu_2+\nu_3-\nu_2$, respectively, and to the inclusion, whenever possible, of higher order hot bands involving the (1,0,0), (0,2,0) and (0,0,1), (1,1,0), (2,0,0) or (0,0,2) states as lower states. Also, the $\nu_1+\nu_3$ linelist was improved for high rotational quantum numbers and the ν_3 and $\nu_1+\nu_3$ bands for $^{15}N^{16}O_2$, which is the second most abundant isotopologue of NO_2, are now included in the database. Finally several weak cold bands in the 2.2 to 4.9 μm region were added for the first time to the GEISA linelist. These new vibration rotation transitions were generated using existing literature data or making use of experimental data extracted from high resolution Fourier transform spectra recorded at SOLEIL for the purpose of this study. One outcome of this study was the first identification of the $\nu_1+2\nu_3-\nu_3$ hot band, leading to the first determination of the (1,0,2) energy level parameters. Also, an improved set of parameters was derived for the (0,1,1) state. The validation of the GEISA-19 linelist was performed through a detailed comparison at 296K between computed and observed Fourier transform laboratory spectra. Also, the consistency, from one band to another, of the energy levels values was carefully checked. Finally inter-comparisons and verifications were performed using the recent versions of the HITRAN (https://hitran.org/) and HITEMP databases [R.J. Hargreaves, I. E. Gordon, L. S. Rothman, S. A. Tashkun, V. I. Perevalov, A. A. Lukashevskaya, S. N. Yurchenko, J. Tennyson, and H. S.P. Müller. *J. Quant. Spectrosc. Radiat. Transf.* **232** 35 (2019)]. Our conclusions are that, at 296K, GEISA-19 is of better quality than HITRAN2016-updated or HITEMP in the overall 1153- 4775 cm^{-1} spectral region. As compared to its previous version, this new linelist will lead to an improved quality of the NO_2 retrievals that will be performed for the future IASI-NG (Infrared Atmospheric Sounding Interferometer New Generation) satellite instrument (https://iasi-ng.cnes.fr/fr). However, contrary to HITEMP, GEISA-19 which does not include transitions involving high rotational quantum numbers or belonging to very high order hot bands cannot be used for hot temperature conditions.

I. Introduction

Because of its important role in the photochemistry of the atmosphere, nitrogen dioxide has been the subject of numerous spectroscopic studies. These led to the generation of linelists which are now included in the GEISA [1], HITRAN [2], and HITEMP [3] databases.

Until very recently (2016), the linelists present in the 2016 version of HITRAN [2] and in the 2015 version of GEISA [1] for nitrogen dioxide did not differ significantly. This 2015 version of the NO_2 linelist, which concerns only the $^{14}N^{16}O_2$ isotopomer, will be noted as "HITRAN-GEISA-15" in the rest of the text. For the $^{14}N^{16}O_2$ species, four spectral regions are considered in HITRAN-GEISA-15 which correspond to the microwave to far infrared region (pure rotation within the (0,0,0) state), the 13.3 μm (ν_2 band), the 6.2 μm (the strong ν_3 band and the weaker ν_1 and $2\nu_2$ dark resonating bands) and 3.4 μm (the rather strong $\nu_1+\nu_3$ band and the weaker $\nu_1+2\nu_2$ dark resonating band) regions, respectively. Together with these cold bands, the HITRAN-GEISA-15 list includes in all four regions lines from the first hot bands which involve the (0,1,0) state as lower vibrational state. These linelists were generated at different time, and with different accuracy, and as it will be discussed in this paper, HITRAN-GEISA-15 presents clear deficiencies.

The most recent version of the HITEMP ("HIgh-TEMPerature molecular spectroscopic database") linelist includes NO_2 for the first time [3]. The aim of HITEMP is to model gas phase spectra for high-temperature applications. For NO_2, a composite HITEMP linelist was generated in the 0- 4775 cm^{-1} by extending the current HITRAN linelist [2] (here labelled as HITRAN2016-updated")[1] using inputs from the recent "Nitrogen Dioxide Spectroscopic Databank" (NDSD-1000) [4,5] line list. These additional inputs concern all spectral regions except the pure rotations bands (microwave to far infrared). For the vibrational transitions already considered in HITRAN, the NDSD-1000 has provided extension of the current list up to the higher N ($N \leq 100$) and K_a values. HITEMP also includes linelists for several cold and hot

[1] In this paper, the reference date for the « HITRAN2016-updated" is September 2020.

bands[2] which, up to now, were missing in HITRAN-GEISA-15. Up to now, HITEMP does not include linelists for the $^{15}N^{16}O_2$ (second) isotope species of nitrogen dioxide.

Subsequently, the "HITRAN2016-updated", the 2020 version of HITRAN, was created [6]. The 1153-4775 cm^{-1} spectral range now include lines from several weaker vibration-rotation bands present in HITEMP which were not considered previously in HITRAN-GEISA-15 [1,2]. More recently, the spectral range for NO_2 has been extended to include transitions between 5720-8000 cm^{-1}, with the addition of several combination and overtone bands [7-&15]. Finally, HITRAN2016-updated now includes line parameters for the ν_3 band of $^{15}N^{16}O_2$ [16] which is the most abundant daughter isotopologue of NO_2.

Therefore, as compared to the previous version of HITRAN [2], both HITRAN2016-updated and HITEMP [3] databases were significantly extended. However, the existing deficiencies in HITRAN-GEISA-15 were not corrected.

The purpose of the present work was to generate a new version of GEISA linelist for NO_2, here identified as 'GEISA-19", which now includes NO_2 lines parameters for the 0 – 4775.3 cm^{-1} region.[3] As far as the line positions and intensities are concerned, this update does not concern the microwave to far infrared region, while all other spectral regions took benefit of new parameters generated during this work.

For the 6.2 μm and 3.4 μm regions which correspond to the strongest NO_2 infrared absorption, we process to the replacement of the cold and of «first» hot bands, and GEISA-19 now includes, when possible, line parameters from higher order hot bands. We also implement in GEISA-19 linelists for several weak cold bands that absorb in the 2000- 4775 cm^{-1} spectral range. In addition, GEISA-19 includes linelists for the ν_3 and $\nu_1+\nu_3$ bands for the $^{15}N^{16}O_2$ isotopic species.

Therefore, it is clear that the GEISA-19 linelist differs from HITRAN-GEISA-15, HITRAN2016-updated [6], and HITEMP [3].

The present work was performed using, as input to our calculations, not only the spectroscopic data available in the literature but also additional data issued from two recent spectroscopic

[2] In the rest of the paper, we will designate as "first", "second", "third" and "fourth" hot bands the vibrational bands involving, as lower vibrational state, the (0,1,0) state, one of the states belonging to the first triad {(1,0,0),(0,2,0),(0,0,1)}, second triad {(1,1,0),(0,3,0),(0,1,1)}, or first hexade {(2,0,0),(1,2,0),(1,0,1), (0,4,0), {(0,2,1), (0,0,2)} of interacting states of NO_2, respectively.

[3] This work does not concern 4800-8000 cm^{-1} spectral range which is now considered in HITRAN16-updated.

studies (Refs. [17] and [18]), or obtained from the analysis of two new FTS spectra recorded during this work.

Before going into detail description of the work, we will define the vibrational and rotational quantum numbers and the energy levels used in this paper. Then we will describe the theoretical models used for the computations.

II General considerations

II-A The NO_2 vibrational and rotational quantum numbers

Nitrogen dioxide ($^{14}N^{16}O_2$) is an asymmetric rotor, with three vibrational modes, ω_1, ω_2, which are symmetric and ω_3 which is antisymmetric, and the vibrational modes are noted as (v_1,v_2,v_3). As a matter of consequence, the vibrational states are grouped in polyads of interacting states. When necessary, the rovibrational interactions were accounted for in order to reproduce the measured line positions and intensities, and the present computations were performed polyad by polyad.

This molecule possesses an unpaired electron, and the electron spin-rotation interaction causes a doublet structure which is usually observable in the infrared. In addition, the hyperfine structure due to the I=1 nuclear spin is observable in the microwave, far infrared and 13.3 μm regions [19, 20]. This work deals with the computation of line positions and intensities in the 1000- 4775.3 cm^{-1} spectral range. Therefore, only four (N, K_a, K_c, and J) rotational quantum numbers are considered for the upper and lower energy levels. The N, K_a and K_c are the main rotational quantum numbers. Because the electronic spin-rotation interaction has to be considered, the J quantum number (associated to **J**=**N**+**S** (with S=±1/2)) is indicated by a "+" and "-" flag.

II B Definition of the upper E_U and lower E_L state energy levels.

Each given vibration spin-rotation transition located at a σ position is then identified by its $\left(v_1^U, v_2^U, v_3^U\right)\left\lfloor N^U, K_a^U, K_c^U, J^U\right\rfloor$ and $\left(v_1^L, v_2^L, v_3^L\right)\left\lfloor N^L, K_a^L, K_c^L, J^L\right\rfloor$ upper and lower state vibration and rotational quantum numbers. For each considered transition, the HITRAN-GEISA-15, HITRAN2016-updated and HITEMP databases include the value of the lower state energy, E_L, while the upper level energy, E_U, is easily computable from the position, σ of the

considered transition (E_U=E_L+σ). Within these databases one should expect that the individual values of E_L (resp. of E_U) should be consistent from one given vibration –transition band to the other one, provided that they involve the same lower $\left(v_1^L, v_2^L, v_3^L\right)\left\lfloor N^L, K_a^L, K_c^L, J^L\right\rfloor$ (resp. same upper $\left(v_1^U, v_2^U, v_3^U\right)\left\lfloor N^U, K_a^U, K_c^U, J^U\right\rfloor$) vibrational spin-rotational level.

III Line position, line intensity and line shape parameters

During this work the linelists for numerous vibration – rotation bands were generated in the 1153- 4775.4 cm^{-1} spectral region, and the theoretical models used to compute the line positions and intensities account both for the spin- rotation resonances and for various vibration – rotational resonances.

III-A Line positions

For the computation of the energy levels, the Hamiltonian matrix involves in its v-diagonal blocks the sum of Watson's type rotational [21] and of electronic spin rotational interaction operators [22]. These v- type operators are written for an A-type reduction and in an I^r representation. The $\left(v_1, v_2, v_3\right) \Leftrightarrow \left(v_1', v_2', v_3'\right)$ v- off diagonal operators are Fermi-type or C-type Coriolis operators, for $|\Delta v_3|$=even and $|\Delta v_3|$=odd, respectively. Starting with the first triad of interacting states {(1,0,0),(0,2,0),(0,0,1)}, strong second order C-type Coriolis resonances are coupling together the spin-rotational levels of the (v_1, v_2, v_3±1) and (v_1, v_2 ±2, v_3) vibrational states. In addition, a first order C-type Coriolis resonance may have to be accounted for the (v_1 ±1, v_2, v_3±1) and (v_1, v_2, v_3) resonating energy levels involving rather high K_a values [23, 18].

In the rest of the paper, the generic term "energy level parameters" will designate the set of vibrational energies, rotational, spin- rotation, and coupling constants which are associated to a given block of interacting vibration states of NO_2.

Several of the computations performed during this study were done using the energy level parameters quoted in the literature, and the form of the Hamiltonian matrices used during these calculations are explicitly described in the attached papers. However, during this work we could make use of new FTS spectra recorded at 6.3 μm and 4.8 μm during this work and of a spectrum recorded at 3.4 μm in Ref. [18] which allowed a detailed investigation of several hot bands. Using these results, we could perform an update of the energy level parameters for the {(0,3,0),(0,1,1)} interacting states and generate the first existing set of energy level parameters

for the {(1,2,1),(1,0,2)} interacting states. The Hamiltonian matrices used during these two computations are given in Table 1.

III-B Line intensities

A detailed description of the method which is used to compute the NO_2 line intensities was given in Refs. [23, 24]. The intensity, $k_{\tilde{\nu}}^{N}(T)$, of a line of a pure $^{14}N^{16}O_2$ isotopic sample is given (in $cm^{-1}/(molecule \times cm^{-2})$) by :

$$k_{\tilde{\nu}}^{N}(T) = a_{iso}\frac{8\pi^3\tilde{\nu}}{4\pi\varepsilon_0 3hc}\exp\left(-\frac{E_L}{kT}\right)\left(1-\exp\left(-\frac{\tilde{\nu}}{kT}\right)\right)\frac{g_L}{Z(T)}R_L^U \quad \text{Eq.(1)}$$

In this expression, a_{iso} is the isotopic concentration of the considered isotopic species (a_{14}=0.991616 and a_{15}=0.00364 for $^{14}N^{16}O_2$ and $^{15}N^{16}O_2$, respectively [25]). $\tilde{\nu} = (E_U - E_L)/hc$ is the wavenumber of the transition, and E_L and E_U are the energies of lower and upper levels of the transition (in cm^{-1}). The total partition function, $Z(T) = Z_{vib}(T) \times Z_{rot}(T)$, is $Z_{14}(296\ K)$ = 13618 for $^{14}N^{16}O_2$ which includes the nuclear spin contribution ($g_{Nuclear}^{14} = 2I+1 = 3$) (resp. $Z_{15}(296\ K)$=9324.7, and $g_{Nuclear}^{15} = 2I+1 = 2$, for $^{15}N^{16}O_2$).

Finally, R_L^U is the square of the matrix element of transformed transition moment operator for the considered band. Let us remind that, as for line positions, the intensity computations account of the vibration-rotation resonances, of the centrifugal distortion effects, and of the electron-spin rotation resonances.

For the line intensities of the strong ν_3 band at 6.2 μm and for the rather strong $\nu_1+\nu_3$ at 2.3 μm of $^{14}N^{16}O_2$ and $^{15}N^{16}O_2$ we used the expansion of the transition moment parameter given in Ref. [23] and Ref. [26], respectively. For the transition moment operators of the hot bands associated to ν_3 and $\nu_1+\nu_3$ bands, at 6.2 μm and 2.3 μm, we used the harmonic approximation, which leads to:

$$^{(v_1,v_2,v_3+1)(v_1,v_2,v_3)}\mu'_Z = \sqrt{v_3} \times {}^{(0,0,0)(0,0,1)}\mu'_Z \quad \text{Eq. (2-a)}$$

and

$$^{(v_1,v_2,v_3)(v_1+1,v_2,v_3+1)}\mu'_Z = \sqrt{v_1 \times v_3} \times {}^{(0,0,0)(1,0,1)}\mu'_Z \qquad \text{Eq.(2-b)}$$

During this work, several weak cold bands were also considered for GEISA-19, and details on the line intensity parameters that we used for these bands are given in the text.

III-C Line shape parameters

In Ref. [27], Benner *et al.* measured a very complete set of accurate line shape parameters for the ν_3 band of NO_2. Following these results, polynomial expansions in 'm' ($m=N_{lower}$ for P or Q lines, and $m= N_{upper}$ for the R transitions) were proposed for the air-broadening linewidths (γ_{Air}) and their associated "n"- temperature dependences and for the pressure shift (δ^0) parameters.

The polynomial expressions achieved for γ_{Air} and "n" in Ref. [27] for the ν_3 band were implemented for all vibrational bands in the GEISA-19 database. This means that we assume that the vibrational dependence of γ_{Air} and "n" is negligible. More precisely, the air broadening linewidths (γ_{Air}) were computed using the 'm' polynomial expressions that are quoted for K_a=0 to K_a=8 in Figs. 5 of Ref. [27], and for larger K_a values (K_a >8) we used the K_a=8 expression. These polynomial expressions can lead, for large "m" values, to unreasonably weak values for γ_{Air} : in such conditions, we fixed γ_{Air} to a default value ($^{Default}\gamma_{Air}$ =0.06 cm^{-1}/atm) which corresponds to the asymptotic behaviour of the plots presents on Figs. 5 of Ref. [27]. For the air broadening associated "n"- temperature dependences, we used the expression quoted in Fig. 8 of Ref. [27].

As far as the δ^0 pressure shifts are concerned, we used the "m"- expansions given on Fig. 9 of Ref. [27] for the ν_3 bands of the $^{14}NO_2$ and $^{15}NO_2$ species, while for other vibrational bands, the pressure shifts were set to a (default) zero value. This is because it was established that the results on pressure shifts for the ν_3 band are not transferable to any other vibrational band [28]. Finally, the default value γ_{Self}=0.095 cm^{-1}/atm [29] was set up for the self-broadening parameters.

This strategy clearly differs clearly from the one which was adopted in HITRAN2016-updated and HITEMP, where a vibrational dependence of the air- broadening and self linewidths, of the "n"- temperature dependence of air- broadening linewidth, and of the pressure

line shift parameters was computed (see Ref. [3] and Ref. [5] and references therein), starting from the experimental results of Ref. [27].

Therefore, our computed line shape parameters differ from those quoted in HITEMP and HITRAN2016-updated.

IV. Experimental details

Three high-resolution absorption spectra (FTS12, FTS3 and FTS3bis) of nitrogen dioxide were recorded on the Bruker IFS125HR Fourier transform spectrometer of the AILES Beamline at Synchrotron SOLEIL, coupled to the newly developed corrosive gas multipass cell [30] set to a 10.88 m path length. For the spectrum in the $\nu_1+\nu_2$ region, (FTS12) the cell path length was set to 10.88 m, the interferometer was equipped with a Si/CaF_2 beam splitter and an InSb detector. The spectral resolution was chosen to give an apparatus function (0.0028 cm^{-1}) smaller than the Doppler width (ca. 0.0048 cm-1) in the considered spectral domain. The instrument was operated with a 1.3mm diameter entrance aperture and a quartz-halogen source, as the synchrotron source presents no advantage at this resolution in this spectral domain. For the second spectrum, in the ν_3 region, (FTS3 and FTS3bis), the cell path length was set to 2.72m and a Ge/KBr beamsplitter, a home-made 4K-cooled HgCdTe with a 1180-1880 cm^{-1} cold band pass filter and 1.2 mm aperture [31] were used. The instrument was operated with a 1.3mm aperture and at 0.002cm^{-1} resolution, well below the Doppler width. The spectrometer was evacuated to about 5×10^{-5} hPa in order to minimize H_2O and CO_2 absorptions. Spectra were ratioed against single channel background spectra of the empty cell, recorded at a resolution of 0.04 cm^{-1} in order to ensure the best possible signal-to-noise in the ratioed spectrum. For the Fourier transform, a Mertz-phase correction with 2 cm^{-1} phase resolution, a zero-filling factor of 2 and no apodization (boxcar option) were applied to the averaged interferograms (880 scans). The spectra were calibrated with residual CO_2 or H_2O lines observed in the spectra with their wavenumbers taken from HITRAN database [2]. The standard deviation after calibration with well isolated reference gas lines is 0.00005 $cm^{-1}(1\sigma)$. Thus, the estimated frequency accuracy of our measured lines is thus close to the lines reported accuracy (0.0001 cm^{-1}), estimated to be 0.0002 cm^{-1}.

The NO_2 gas bottle used (Sigma-Aldrich, France 99.5%) was found to contain NO, N_2O and other impurities at a much higher level than the stated purity. It was then first purified following the standard procedure [23] by pumping on the frozen solid at about 200K until the bluish colour due to N_2O_3 disappeared. This eliminated most of the impurities. We thus added a further step by letting 5 mmoles of the gas mixture react with about 0.5 mmole of ozone, prepared separately from 99.999% pure O_2. The remaining ozone and oxygen were removed by pumping above the mixture re-cooled to about 210K. This successfully removed the NO and N_2O traces. The total pressures were measured using a Pfeiffer 10 hPa capacitive gauge. A small contamination due to CO_2 remained visible, but could be estimated to about 0.2% of the gas sample, using IR integrated intensity measurements.

In the near infrared, $\upsilon_1+\upsilon_2$ region, the sample gas pressure used was 5.1± 0.1 hPa. Assuming a negligible contribution of foreign gases, the total pressure can be attributed to the mixing of the monomer (NO_2) and dimer (N_2O_4) forms of nitrogen dioxide. These two forms exist in equilibrium, according to the equation ($2NO_2 \leftrightarrow N_2O_4$), with:

$$P^2(NO_2) = K_P\, P(N_2O_4) \qquad \text{Eq. (3)}$$

where K_P is the equilibrium constant between NO_2 and N_2O_4, whose value depends on temperature [32] (at 296K, $K_p = 123.3$ hPa) $P(NO_2)$ and $P(N_2O_4)$ are the partial pressures of the monomer and dimer, respectively. In such conditions, the monomer (NO_2) and dimer (N_2O_4) partial pressures can be estimated in the at about $P(NO_2) \approx 4.9\pm 0.1$ hPa, $P(N_2O_4) \leq 0.2$ hPa. For the second (FTS3) and third (FTS3bis) spectra, in the ν_3 mid-infrared range, the sample gas pressure was much lower, (0.20 hPa and 0.62 hPa, respectively) and although N_2O_4 is detectable, due to the long optical path length its partial pressure can be estimated to be quite low, on the order of 0.001 hPa and 0.003 hPa, respectively.

Fig. (A1) and (A2) give overviews of the FT3 and FT12 spectra. While saturated in its central part, the FTS3 and FRS3bis spectra were used in its P branch to identify lines belonging to hot bands and test the quality of the GEISA-19, HITRAN2016-updated, and HITEMP databases. The FTS12 spectrum corresponds to the B-type $\nu_1+\nu_2$ band.

Also, we used FTS spectra, or portions of spectra, recorded during previous NO_2 investigations. Table 2 summarizes the information on these spectra (FTS13, FTS23. FTS33, FTS113 and FTS333) which are associated to the investigation of the $2\nu_1$ and $\nu_1+\nu_3$ bands [18],

the $\nu_2+\nu_3$ band [29], the $2\nu_2+\nu_3$, $4\nu_2$, and $2\nu_3$ [34] interacting bands, and the $2\nu_1+\nu_3$ and $3\nu_3$ bands [35]. All spectra were recorded on Bruker instruments, type IFS125HR (FTS12, FTS3, FTS3bis, FTS13) or FTS120HR (other spectra), at a resolution ranging as R=0.002 - 0.003 cm^{-1}, and at room temperature conditions.

Some additional comments concern spectra FTS113 and FTS333 which were used to perform the most recent line positions and (relative) line intensities investigations for the $2\nu_1+\nu_3$ and $3\nu_3$ bands of NO_2 [35]. Hargreaves et al. [3] pointed out that the experimental intensities measured for these two bands in Ref. [35] lead to cross sections which are, on the average, 3.5 times weaker than those delivered at 25°C by the Pacific Northwest National Laboratory (PNNL) [36]. At the present time we decided to adopt the strategy suggested by Hargreaves et al. [3], this means that in GEISA-19, the intensities of the $2\nu_1+\nu_3$ and $3\nu_3$ bands were calibrated on the absolute scale using the PNNL cross sections.

V The GEISA-19 database in the far infrared and 13.3 µm region, and status of the energy parameters for the (0,0,0), (0,1,0) and {(1,0,0),(0,2,0),(0,0,1)} states of $^{14}N^{16}O_2$:

V-A The microwave to far infrared region and the 13.3 µm regions.

In HITRAN-GEISA-15 the microwave and far infrared region, involves rotational transitions within the (0,0,0) and (0,1,0) vibrational state [19,20, 37]. The 13.3 µm region considers the lines belonging to the ν_2 band [20] and its associated $2\nu_2$-ν_2 «first» hot band [33, 20]. The details on the line intensities calculations, models and parameters, are given in Refs. [19] [20] and [33]. As far as the line positions and intensities, these microwave to far-infrared and 13.3 µm linelists were not updated during the present work because we do not have any new spectroscopic data or a new model which encourage us to perform such modification.

V-B Status of the (0,0,0), (0,1,0) and {(1,0,0),(0,2,0),(0,0,1)} energy levels parameters

At this level, it is necessary to justify the choice of the energy level parameters used during this work for the computation of energy levels of the (0,0,0), (0,1,0) vibrational states and for those of the first triad of {(1,0,0),(0,2,0),(0,0,1)} interacting states.

The (0,0,0), (0,1,0) vibrational states

During the present update of GEISA-19 we used the (0,0,0) and (0,1,0) energy level parameters quoted in Ref. [37] and [20], respectively, for the whole set of line position computations. These parameters were derived from combined fits of experimental data extracted from high resolution Fourier transform infrared spectra and from microwave measurements. Indeed those (0,0,0) and (0,1,0) energy level parameters are significantly more accurate than those quoted in Ref. [38]: at that time the investigation was performed using infrared grating spectra or diode laser measurements, and the spin- rotation resonances were accounted only through second order perturbation.

The {(1,0,0),(0,2,0),(0,0,1)} interacting states:

As far as the {(1,0,0),(0,2,0),(0,0,1)} energy levels are concerned, the $2\nu_2$-ν_2 linelist at 13.3 μm is not consistent with the ν_1, $2\nu_2$, and ν_3 linelist at 6.2 μm. This is because two different sets of energy level parameters, Ref. [33] at 13.3 μm, and Ref. [23] and 6.2 μm, were used at the computation of the upper state energy levels. Historically, a first set of energy level parameters for the first triad of $^{14}NO_2$, was obtained in Ref. [23] using as input to the least squares fit calculation experimental energy levels for the {(1,0,0),(0,2,0),(0,0,1)} interacting states that were obtained during the investigation of high-resolution FTS spectra at 6.2 μm. At that time, the identification of the ν_1 and ν_3 bands was very extended, while for $2\nu_2$, only several series were observed, which involves for the (0,2,0) vibration state only the K_a=0-2 and K_a=6 rotational quantum numbers. The additional missing information for the K_a=3,4 and 5 series of (0,2,0) could be filled through the latter identification of the $2\nu_2$-ν_2 hot band in high resolution spectra recorded at 13.3 μm [33]. Therefore, in Ref. [33] the energy levels parameters for the first triad of $^{14}NO_2$ were refined during a least squares fit which combined together the experimental spin- rotation energy levels of the (0,0,1), (1,0,0) and (0,2,0) states originating from both analyses, at 6.2 μm [23], and at 13.3 μm [33]. This justify the choice of the parameters of Ref. [33] rather than those of Ref. [23] for the computations the (0,0,1), (1,0,0) and (0,2,0) upper or lower state energy levels in the whole GEISA-19 database.

VI The GEISA-19 database in the 1153-4775 cm^{-1} spectral region

For wavenumbers greater than 1153 cm^{-1}, GEISA-19 was largely modified as compared to its previous version. First, we updated the lists for the main cold bands and the first hot bands

which were the only originally present in HITRAN-GEISA-15 at 6.2 and 3.4 µm. Also, we add new linelists which concern (i) higher order hot bands in the 6.2 µm and 3.4 µm regions (ii) several weaker bands in the 2.3 to 4.9 µm region, and (iii) the ν_3 and $\nu_1+\nu_3$ bands for the $^{15}N^{16}O_2$ isotopic species of nitrogen dioxide.

For GEISA-19, we tried to generate accurate vibration- rotation bands each time this proved to be "technically possible". The limitation concerns the quality of line position and line intensity parameters that we had at our disposal. For example, the very weak $\nu_1+2\nu_3$ weak cold band at 2.2 µm, present in HITRAN-2016 and HITEMP, is absent in GEISA-19 because we do have at our disposal intensity parameters for this band. Contrary to HITEMP, GEISA-19 does not includes lines involving very high rotational quantum numbers, and numerous higher order hot bands are missing.

VI-A Updates of the lists included in HITRAN-GEISA-15

V-A-1 The cold bands in the 6.2 µm and 3.4 µm regions for $^{14}N^{16}O_2$.

The 6.2 µm bands

For GEISA-19 a new linelist was generated for the ν_1, $2\nu_2$, and ν_3 interacting bands at 6.2 µm using the energy level parameters of Ref. [33]. Let us mention that the ν_3 and ν_1 bands are only weakly affected in this new calculation as compared to the previous linelist [39]. In fact, only the very weak K_a=3-5 series, or those with $K_a \geq 7$ of the dark $2\nu_2$ band have their positions significantly modified.

The 3.4 µm bands:

The recent update of the $\nu_1+\nu_3$ band at 3.4 µm was presented in details in Ref. [18]. Let us recall that this recent analysis unable to assign $\nu_1+\nu_3$ lines up to N=75 and K_a= 14 (instead of N= 55 and K_a= 10, in Ref. [26]). In addition, a new investigation of the $2\nu_1$ band was performed. The energy level computation involves six interacting states {(2,0,0),(1,2,0),(1,0,1), (0,4,0),(0,2,1),(0,0,2)}, instead of two {(1,2,0),(1,0,1)} previously [26]. Also, detailled line intensity measurements and calculations were performed for the $2\nu_1$ band [18]. Indeed, this band exibits an "unusual" intensity behaviour for a B-type band, with, for example, a very weak P- branch. The progress achieved for the $\nu_1+\nu_3$ and $2\nu_1$ linelists [18] as compared to their counterparts in HITRAN2016-updated [6] and HITEMP [3] are resumed shortly latter in the text.

VI-A-2 The "first" hot bands in the 6.2 μm and 3.4 μm regions for $^{14}N^{16}O_2$.

We will present the updates performed for the "first" hot bands associated to the strongest absorbing bands of NO_2 in the 6.2 μm and 3.4 μm regions.

The 6.2 μm bands and update of the energy level parameters for the {(0,3,0),(0,1,1)} interacting states.

As far as the line positions are concerned, the list for the $\nu_2+\nu_3-\nu_2$ hot band present in HITRAN-GEISA-15 was generated using for the {(0,3,0),(0,1,1)} upper and (0,1,0) lower states the energy level parameters quoted in Ref. [38]. Let us remind that these parameters were achieved using a composite set of experimental data (grating and diode laser spectra). In addition, the spin- rotation resonances were only accounted for through a second order treatment. This $\nu_2+\nu_3-\nu_2$ list, which is unchanged in HITRAN2016-updated, was only extended in HITEMP up to higher values of the N and K_a rotational quantum numbers.

For the preparation of GEISA-19 we generated a new version of the linelist for this hot band. In a preliminary step, the line positions were computed using the upper and lower state energy level parameters of Refs. [29] and [20] for the {(0,3,0),(0,1,1)} and (0,1,0) states, respectively. The comparison between calculated spectrum and the observed one (the FTS3 or FTS3bis spectra in the P branch region) proved that this preliminary $\nu_2+\nu_3-\nu_2$ linelist was already more precise than the existing one in HITRAN-GEISA-15, although not perfect. Indeed, we notice that the $\nu_2+\nu_3-\nu_2$ transitions involving high K_a values ($11 \geq K_a \geq 9$) differ from their predicted positions. We used these $\nu_2+\nu_3-\nu_2$ new assignments to generate an additional set of 37 experimental spin-rotational energy levels for the (0,1,1) state by adding the $\nu_2+\nu_3-\nu_2$ line positions to the calculated (0,1,0) state energy levels [20]. These additional set of (0,1,1) levels were combined with those already measured during the investigation of the $\nu_2+\nu_3$ band [29], and these data were introduced in a least squares fit calculation to get refined values for the {(0,3,0)(0,1,1)} interacting states parameters. These constants which are given, together with their associated uncertainties in Table 3, were used to generate the final linelist for the $\nu_2+\nu_3-\nu_2$ band which is quoted in GEISA-19.

The list of assigned $\nu_2+\nu_3-\nu_2$ transitions involving high K_a values ($11 \geq K_a \geq 9$), and the results of the energy level computation for the {(0,3,0)(0,1,1)} state are given in the Supplementary data of this article.

The 3.4 μm bands:

In HITRAN2016-updated the list for the $\nu_1+\nu_2+\nu_3-\nu_2$ band, located at 2888.191 cm^{-1}, coincides with HITRAN-GEISA-15's. This list, which is restricted to the 2850.082 - 2917.363 cm^{-1} spectral region, was generated using for the energy positions in the upper {(1,2,0),(1,1,1)} and lower (0,1,0) states the parameters quoted in Ref. [40] and [38], respectively. As for its $\nu_2+\nu_3-\nu_2$ counterpart at 6.2 μm, this list is not very accurate for the same reasons (low quality of the theoretical model and of the experimental data used as input to the calculation). For HITEMP the $\nu_1+\nu_2+\nu_3-\nu_2$ linelist was extended to include lines involving higher N and Ka values.

For GEISA-19, the generation of the new linelist for the $\nu_1+\nu_2+\nu_3-\nu_2$ band was performed using for the line positions the upper {(2,1,0),(1,3,0),(1,1,1)} and lower (0,1,0) energy level parameters collected in Ref. [17] and [20], respectively.

VI-B New input in GEISA-19: higher order hot band in the 6.2 μm and 3.4 μm regions

VI-B-1 Higher order hot bands in the 3.4 μm region, and first investigation of the $\nu_1+2\nu_3-\nu_3$ hot band:

In the 3.4 μm region, the three stronger second order hot bands are the $2\nu_1+\nu_3-\nu_1$, $\nu_1+2\nu_3-\nu_3$, and $\nu_1+2\nu_2+\nu_3-2\nu_2$ hot bands, located at (about) 2860.144, 2844.218 and 2870.76 cm^{-1}, with a relative intensity at 296K of 0.32%, 0.077%, and 0.065%, respectively as compared to the cold $\nu_1+\nu_3$ band (located at 2906.074 cm^{-1})

It was rather easy to generate a linelist for the $2\nu_1+\nu_3-\nu_1$ band using for the computation of the upper and lower state levels the energy level parameters of Refs [35] and [33], respectively. In this way, lines of the $2\nu_1+\nu_3-\nu_1$ hot band could be identified in the FTS13 spectrum within strong lines of the P branch of the $\nu_1+\nu_3$ band

On the other hand, the situation for the $\nu_1+2\nu_3-\nu_3$ and $\nu_1+2\nu_2+\nu_3-2\nu_2$ hot bands was not so simple since, to our knowledge, the very weak $\nu_1+2\nu_3$ and $\nu_1+2\nu_2+\nu_3$ bands were never investigated at high or medium resolution. The only existing information concerns the band centers which were measured by laser fluorescence spectroscopy [41] at 4461.07 and 4369.10 cm^{-1} for the (1,0,2) and (1,2,1) vibrational states.

Therefore, the right method was to try to identify these hot bands in the congested FTS13 spectrum which was recorded for a large (pressure ×path length) product (see Ref. [18]),

because numerous lines were unidentified at that time. To solve this problem, we generated predictive line lists for the $\nu_1+2\nu_3-\nu_3$ and $\nu_1+2\nu_2+\nu_3-2\nu_2$ bands.

We were unfortunately not able to identify the $\nu_1+2\nu_2+\nu_3-2\nu_2$ band which is located in a congested part of the FTS13 spectrum. Fortunately, we were luckier for the $\nu_1+2\nu_3-\nu_3$ hot band, as the line prediction helped us to perform several assignments. The calculated (0,0,1) state energy levels [33] were added to the first observed $\nu_1+2\nu_3-\nu_3$ line positions to get a preliminary set of (1,0,2) experimental spin-rotational energy levels. These upper state levels were then introduced in a least squares fit calculation to get refined values for the {(1,0,2)(1,2,1)} energy level parameters, and therefore perform new assignments, and then improve the accuracy of the parameters, allowing then further new assignments. This iterative process was performed until no further assignments of $\nu_1+2\nu_3-\nu_3$ lines could be possible. Altogether, about 550 lines (resolved or unresolved spin doublets) were assigned with K_a and N values such that ($0 \leq K_a \leq 8$) ($0 \leq N \leq 45$), leading to the determination of 394 energy levels of the (1,0,2) state.

The final set of vibrational energies, spin rotation, rotational and interacting constants for the {(1,0,2)(1,2,1)} interacting states are collected in Table 3. During this computation, the E_v (vibrational energy) of the (1,2,1) was maintained at the value proposed by Delon and Jost [41] (E_{121}= 4369.10 cm^{-1}). The E_V value of the (1,0,2), E_{102}= 4460. 8648 ± 0.0003 cm^{-1} is in reasonable agreement with the laser fluorescence value proposed by Delon and Jost [41] (E_{102}= 4461.07 cm^{-1}). We also notice that the K_a=4 levels of the (1,0,2) state are resonating with K_a=5 levels of (1,2,1), and that the mixing of the energy levels grows up to 44% for N=44. We used these energy level parameters together with the first triad constants of Ref. [33] to generate the line positions of the $\nu_1+2\nu_3-\nu_3$ hot band. The associated intensities were computed using the method described previously.

The complete list of assignments and the results of this calculation are provided as supplementary data of this article.

VI-B-2 Higher order hot bands in the 6.2 μm region

In the 6.2 μm region, the second order hot bands which lead to relative strong contributions are those associated to $|\Delta v_3|=1$ i.e. the $2\nu_2+\nu_3-2\nu_2$, $2\nu_3-\nu_3$ and $\nu_1+\nu_3-\nu_1$ hot bands located at 1594.14, 1584.59 and 1586.95 cm^{-1}. The line positions were computed using

the energy level parameters of Ref. [18] and of Ref. [33] for the upper and lower states respectively.

Whenever possible, we generated also higher order hot bands. This was possible in the 6.2 μm region for the $\nu_1+\nu_2+\nu_3-(\nu_1+\nu_2)$, $2\nu_1+\nu_3-2\nu_1$, $\nu_1+2\nu_3-(\nu_1+\nu_3)$ and $3\nu_3-2\nu_3$ hot bands. For the upper state energy levels we used the energy level parameters of the (1,1,1) (Table 3 of Ref. [17]), (2,0,1), and (0,0,3) (Table 3 and 4 of Ref. [35]), and for (1,0,2) those in Table 3 of this work, while for the (1,1,0) and {(2,0,0),(1,2,0),(1,0,1), (0,0,2), (0,4,0),(0,0,2)} states, we used the parameters quoted in Table 1 of Ref. [42] and Table 4 of Ref. [18], respectively.

VI-C New input in GEISA: weak cold bands in the 2.2 to 4.9 μm spectral regions :

The new versions of HITRAN2016-updated [6] and HITEMP [3] databases include linelists for numerous weak bands which were not considered in HITRAN-GEISA-15. For several of these rather dark bands, this is now the case for GEISA-19.

¤ The $2\nu_1$ band centered at 2627.34 cm^{-1} was already the subject of an extensive study (positions and intensities) in Ref. [18], leading to a linelist now included in GEISA-19.

¤ GEISA-19 includes linelists from the $\nu_1+\nu_2$ band [42], $2\nu_2+\nu_3$ and $2\nu_3$ bands [34,14], and $2\nu_1+\nu_3$ and $3\nu_3$ bands [35], located at 2063.12, 3092.48, 3201.44, 4179.94, and 4754.21 cm^{-1}, respectively together with some lines associated to their dark interacting bands. For these bands we used, without modifications, the energy level parameters and the expansion of the transition moment operators which are quoted in the original papers. The only exception concerns the intensities of the $2\nu_1+\nu_3$ and $3\nu_3$ bands which were calibrated relative to the PNNL cross sections for NO_2 [36].

¤ GEISA-19 includes linelists from the $\nu_2+\nu_3$ band located at 2355.15 cm^{-1}. For this computation we used the improved energy level parameters achieved for the {(0,3,0),(0,2,1)} interacting states during this work (see Table 3) for the computation of the (0,1,1) upper levels, and the expansion of the $\nu_2+\nu_3$ transition parameter quoted in Ref. [29] for the $\nu_2+\nu_3$ intensities.

¤ The very weak $\nu_1+\nu_2+\nu_3$ band located at 3637.848 cm^{-1} [17] is not included in HITEMP or HITRAN2016-updated. The FTS123 Fourier transform spectrum used in Ref. [17] was recorded without purification of the NO_2 sample. So, the presence of impurities prevents to use this spectrum for line intensities measurements. However, Fig.1 in Ref. [17] shows that the band intensity pattern of the $\nu_1+\nu_2+\nu_3$ band does not differ from what is expected for a

classical A –type band of nitrogen dioxide, without any significant distortion effect. Therefore, only the first order term in the expansion of the $\nu_1+\nu_2+\nu_3$ transition moment operator is necessary to compute the line intensities for this band. Its value was estimated to be :

$$^{111,000}\mu_1' \approx 0.27 \times 10^{-2} \text{ D } (+/- 20\ \%)\ ^{4}, \qquad \text{Eq.(4)}$$

using the PNNL cross section data [36]. The uncertainty quoted in Eq. (4) is set up according to the noise level (~5.E-22 cm^2/molecule) in the PNNL cross section data.

VI-D New inputs in GEISA-19: The ν_3 and $\nu_1+\nu_3$ bands for $^{15}N^{16}O_2$:

The linelists for the ν_3 and $\nu_1+\nu_3$ bands of $^{15}N^{16}O_2$, located at 1582.1029 and 2858.7088 cm^{-1},[5] respectively, were included in GEISA-19. We used the line positions and intensities gathered in Refs. [16], and [43], respectively. The computed partition functions for $^{15}N^{16}O_2$ at different temperatures (T=50K to T=500K) are also provided as Supplementary data of the present article.

VI-E Final description of the GEISA-19 database in the 1153- 4775 cm^{-1} spectral region:

The GEISA-19 database for nitrogen dioxide is available on the freely accessible https://geisa.aeris-data.fr/ website. Also, in the 1153-4775 cm^{-1} spectral range, which is the object of this study, this linelist is provided as supplementary data of this work. Table 4 gives a global description of this linelist, with, for each vibrational band and isotopic species ($^{14}N^{16}O_2$ and $^{15}N^{16}O_2$), the vibrational assignment, the number of lines, an approximate band center, the wavenumber range (in cm^{-1}), the band intensity and the minimum and maximum values of the individual line intensities intensity (in cm^{-1}/(molecule.cm^{-2}) at 296K), the maximum N values and the range for the K_a rotational quantum numbers in the upper vibrational state.

[4] in Debye (1 D = 3.33564×10^{-30} C m),

[5] The actual band center of the $\nu_1+\nu_3$ band is 2858.7088 cm^{-1} instead of 2858.7077 cm^{-1} in Ref. [43]. Also the Z_{15}(296K)= 9324.7 value was used during the intensities computations for the $\nu_1+\nu_3$ band, instead of the erroneous value "Z_{15}(296K)= 13987" which is quoted in Ref. [43].

It is necessary to estimate the accuracy attached to the computed line positions and intensities. In GEISA-19, each of vibration – rotation linelist was generated through calculations. It is obvious that extrapolations far away from the range of the lower or upper states experimental data used during this computation can be uncertain. To document this point, Table 4 provides for each vibrational band the maximum N value and the K_a range for the upper and lower states experimental energy levels used during the computation.

One can estimate at about 0.001- 0.003 cm^{-1} the accuracy of the line position for transitions involving rotational quantum numbers within the range of the observed energy levels. For transitions outside these limits, the line position accuracy is decreasing with increasing rotational quantum

As far as the line intensities are concerned, the information describing the quality and accuracy of these data are provided in the literature articles which are referred in this paper.

VII-Validations of the new GEISA-19 database.

Two different types of validations for the GEISA-19, HITEMP and HITRAN2016-updated linelists were performed. First the existing laboratory FTS spectra (see Table 2) were used to check these linelists through inter-comparison between observed and calculated spectra. In a second step, we checked, within these databases, the internal consistency of the computed energy levels in term of the Rydberg–Ritz combination principle.

VII-A Validation with the observed laboratory spectra at 296K.

To validate GEISA-19 we compared the calculated and observed spectra using the laboratory FTS spectra at our disposal (see Table 2). The same intercomparison was performed using the HITEMP or HITRAN2016-updated linelist.

VII-A-1 The 6.2 µm region:

We used the FTS3 and FTS3bis spectra recorded during this work to validate our computations.

Figures 1 to 5 detail the computations for several vibrational bands which were computed for GEISA-19 during this work.

Figure 1 presents a portion of the spectrum in the 1557 cm^{-1} region where lines from the $\nu_2 + \nu_3 - \nu_2$ hot band are clearly observable.

Figure 2, 3, and 4 present a portion of the same spectrum in the 1555, 1561 and 1572 cm-1 spectral ranges where lines from the P branches of the $\nu_1+\nu_3-\nu_1$, $2\nu_3-\nu_3$ and $2\nu_2+\nu_3-2\nu_2$ hot bands are clearly visible.

Finally, Figure 5 present a portion of the P- branch of the ν_3 band in the 1559.1 cm^{-1} region. In this case a global comparison GEISA-19 versus HITEMP and HITRAN2016-updated is performed.

VII-A-2 The 2.3 µm region:

For this validation we used the FTS13 spectrum recorded in Ref. [18].

Figures 6, 7, and 8 give portions of FT13 spectrum in the 2838.8 cm^{-1}, 2821.6 cm^{-1} and 2834.8 cm^{-1} spectral ranges, and the comparisons focus specifically on the $\nu_1+\nu_2+\nu_3-\nu_2$, $\nu_1+2\nu_3-\nu_3$ and $2\nu_1+\nu_3-\nu_1$ hot bands, respectively.

Finally, Figure 9 presents a portion of the 2820 cm^{-1} spectral region. In this region, lines from the $\nu_1+\nu_3$ band of $^{15}N^{16}O_2$ are also observable, together with numerous lines from the hot bands from the main species. The comparison of GEISA-19 with HITEMP and HITRAN2016-updated is performed. Note than in HITRAN2016-updated the linelist for the $\nu_1+\nu_2+\nu_3-\nu_2$ hot band is restricted to the 2850.08 -2917.36 cm^{-1} spectral region.

VII-A-3 The weak bands:

During this work several weak bands were added to the GEISA linelist for NO_2.

Fig. 10 presents a portion of the FTS13 spectrum in the 2814.4 cm^{-1} spectral range, where lines from the R branch of the $2\nu_1$ band are easily observable within from those from the P- branches of the $\nu_1+\nu_3$ band and associated hot bands. The agreement (positions and intensities) between the observed and calculated spectra is excellent when using GEISA-20 both for the $2\nu_1$ lines and for the $\nu_1+\nu_3$ band (and for the associated hot bands), while this is not the case for HITEMP. For this figure, Table TA1 (Supp-5 in the supplementary data) provides the assignments, line positions and line intensities for several $^{14}N^{16}O_2$ lines. As far as the $\nu_1+\nu_3$, $2\nu_1+\nu_3-\nu_1$, and $\nu_1+2\nu_3-\nu_3$ (associated hot) bands are concerned, the intensities in HITEMP and

GEISA-20 are in good agreement, while for the $2\nu_1$ lines, the intensities in HITEMP are about two times weaker than in GEISA-20. This is also evidenced on Fig. A9 which presents an overview of the $2\nu_1$ band. Also Fig. A9 in the archive (Supp-5 in the supplementary data) presents an overview of the 2500- 3000 cm^{-1} region of the FTS13 spectrum which corresponds to the $2\nu_1$ and $\nu_1+\nu_3$ bands of $^{14}N^{16}O_2$, it is clear that that HITEMP underestimates the $2\nu_1$ band line intensities by a factor of about two, and that the strange intensity pattern of the $2\nu_1$ band is not accounted for.

For the other weak "cold" bands, the figures presenting intercomparisons are accessible in Supp-5 of the supplementary data of this paper.

Figures A3, A4, A5, A6, A7 and A8 present inter-comparisons for the $\nu_1+\nu_2$ band near 2090.7 cm^{-1} (FTS12), $\nu_2+\nu_3$ band near 2365.2 cm^{-1} (FTS23), $2\nu_2+\nu_3$ band near 3069.68 cm^{-1} (FTS223), $\nu_1+\nu_2+\nu_3$ band near 3650 cm^{-1} (FTS111), $2\nu_1+\nu_3$ band near 4155.2 cm^{-1} (FTS113) and $3\nu_3$ band near 4774.8 cm^{-1} (FTS333).

Except for $\nu_1+\nu_2+\nu_3$, all these weak bands are included in HITRAN2016-updated and HITEMP.

VII-A-4 Conclusion for the intercomparison between observed and calculated spectra:

We notice that the agreement between the observed and calculated spectra is better in all spectral regions when using GEISA-19 rather than with HITRAN2016-updated or HITEMP.

However, the line position differences between databases depend on the considered vibrational transitions.

The ν_3 band was not significantly updated. For the $\nu_1+\nu_3$ band, the most significant discrepancies (more than ~0.01 cm^{-1}) concern lines involving high rotational quantum numbers (K_a= 0 and N ≥69; K_a= 5 and N ≥55; or K_a=10 and N ≥47) [18].

For vibrational transitions involving only excitations in the ν_3 vibrational mode, like the $3\nu_3$ weak cold band at 2.1 μm, the $2\nu_3$-ν_3 and $3\nu_3$-$2\nu_3$ hot bands at 6.2 μm, the differences are in general weaker than for other type of vibrational transitions. However, differences larger than ~0.005 cm^{-1} concern the lines involving N and K_a quantum numbers such that K_a=1 and N ≥35 of $3\nu_3$-$2\nu_3$; K_a=1 and N ≥49 for $2\nu_3$-ν_3 and $2\nu_3$); K_a=1 and K_a=2 and N ≥41 for $3\nu_3$.

More significant discrepencies (larger than ~0.01 cm^{-1}) are observed for the following series (K_a=1 and N ≥23 of $2\nu_1+\nu_3$; K_a ≥5 and N ≥ (50-K_a) or K_a ≥ 9 of $\nu_2+\nu_3-\nu_2$; K_a ≥5 and N ≥

(50-K_a) or $K_a \geq 9$ of $\nu_2+\nu_3-\nu_2$; for $K_a \leq 8$ and $N \geq (42-K_a)$ or $K_a \geq 9$ for $\nu_1+\nu_2+\nu_3-\nu_2$). Let us remind that the $\nu_2+\nu_3-\nu_2$ and $\nu_1+\nu_2+\nu_3-\nu_2$ hot bands give rise to the strongest NO_2 infrared signature in the 6.3 μm and 3.4 μm region after their associated ν_3 and $\nu_1+\nu_3$ associated cold bands.

As expected, larger line position differences (larger than ~0.02 cm^{-1}) between the databases concern bands involving the (2,0,0) or (1,0,2) vibrational states in the upper or lower state of the vibrational transition. However it is clear that these bands are extremelly weak, except for hot bands ($2\nu_1+\nu_3-2\nu_1$, $\nu_1+2\nu_3-2\nu_3$, etc…) for NO_2 spectra in very very high temperature conditions.

VII-B Consistency of the GEISA-19 database for the E_L or E_U as energy levels values (Rydberg–Ritz combination principle).

Within the HITRAN-GEISA-15, HITRAN2016-updated or HITEMP databases one should expect that the individual values of E_L (resp. of E_U) lower (resp. upper) state energy level values to be consistent from one given vibration –transition band to the other one, provided that they involve the same lower $\left(v_1^L, v_2^L, v_3^L\right) \left\lfloor N^L, K_a^L, K_c^L, J^L \right\rfloor$ (resp. same upper $\left(v_1^U, v_2^U, v_3^U\right) \left\lfloor N^U, K_a^U, K_c^U, J^U \right\rfloor$) vibrational spin-rotational energy level. However, this not the case because these linelists were generated by merging numerous unrelated data sources. Table 5 provides several examples of vibration spin- rotation transitions for which this is not the case in HITEMP or HITRAN2016-updated. For example, the computed positions of the (0,2,0) [21,3,19] spin rotational levels are different in the $2\nu_2$, $2\nu_2-\nu_2$, and $2\nu_2+\nu_3-2\nu_2$ bands. This is the case also for the (1,1,0) [42,0,42] or (1,1,0) [33, 1, 33] levels in the $\nu_1+\nu_2$ and $\nu_1+\nu_2-\nu_2$ bands, for the (0,1,1) [31, 9, 22], (0,1,1) [35, 8,27], (0,1,1) [45, 4, 41], or (0,1,1) [27, 10, 17], in the $\nu_2+\nu_3$ and $\nu_2+\nu_3-\nu_2$ bands, or for the (0,2,1) [20,3,18] spin rotational levels in the $2\nu_2+\nu_3$, $2\nu_2+\nu_3-\nu_2$, and $2\nu_2+\nu_3-2\nu_2$ bands. This problem was solved in GEISA-19, and to validate these corrections, Table 5 provides, each time it was possible, the observed line positions which were either observed during previous investigations (see the literature) or identified during the present work.

VII-C Comparison with the PNNL cross-sections.

In Fig. 11, we compared the cross-sections computed using the HITEMP and GEISA-19 linelists with the PNNL NO_2 cross sections [36]. Althought remaining absorption due to the N_2O_4 dimer are quite observable (in the 1263, 1751, 2630 and 2971 cm^{-1} spectral regions) in the PNNL spectra, we can notice the following points.

- In GEISA-19, the $2\nu_1$ band is significantly stronger than in HITEMP, and this is in agreement with the PNNL data.
- GEISA-19 includes data for the $\nu_1+\nu_2+\nu_3$ band at 3637 cm^{-1}, while this linelist is absent in HITEMP.
- HITEMP includes data for the $\nu_1+2\nu_3$ band at ~4500 cm^{-1}, while this linelist is absent in GEISA-19. This is because we do not have reliable intensity data for this very weak band which, in Fig. 11 is masked in the noise level (about 5×10^{-22} cm^2/molecule) of the PNNL cross-section.

Conclusion

During this work, a new version of the line by energy level parameters (line positions, intensities and shape) for nitrogen dioxide was generated for the 0- 4700 cm^{-1} spectral range and implemented in the (Gestion et Etude des Informations Spectroscopiques Atmosphériques) GEISA database (https://geisa.aeris-data.fr/). Except for the far infrared and 13.3 µm regions all spectral regions are significantly affected by this major update.

For the main ($^{14}N^{16}O_2$) isotope species, the updated lists involve the main cold bands (ν_1, $2\nu_2$ and ν_3 and $\nu_1+\nu_3$, respectively) together with their associated «first» hot bands, and, whenever possible, higher order hot bands. One of the outputs of this work was the first identification of the $\nu_1+2\nu_3-\nu_3$ hot band, leading to the first determination of the energy level parameters for the (1,0,2) vibrational state of $^{14}N^{16}O_2$. Also, the quality of the (0,1,1) energy level parameters was improved during the investigation of the $\nu_2+\nu_3-\nu_2$ hot band. In addition, the linelists for several weak cold bands were implemented in GEISA-19 for the first time. For $^{15}N^{16}O_2$, which is the most abundant daughter isotopologue of nitrogen dioxide, we included in GEISA-19 the line parameters for the ν_3 and $\nu_1+\nu_3$ bands.

These new lists, were validated using high resolution Fourier transform spectra recorded at SOLEIL at 296K or during previous laboratory studies. It appeared that, as compared to HITRAN2016-updated and HITEMP, GEISA-19 leads to better agreements between calculated and observed spectra in all spectral regions. In term of line position calculations, GEISA-19 proved to be more consistent than HITRAN2016-updated and HITEMP. However, GEISA-19, which does not include transitions involving very high rotational quantum numbers or belonging to higher order hot bands, is not suitable for uses at high temperatures.

Acknowledgments

The authors acknowledge support from synchrotron SOLEIL (project 99200018). This work was supported by the French National program LEFE « Les Enveloppes Fluides et l'Environnement » through the « MEANSPECFORUM » project. It is also funded by the French National program ANR (ANR-19-CE29-0013) through the « QUASARS » project. Also, we thank the reviewer for his very valuable comments.

APPENDIX-A: description of the supplementary data

Supp-1: The GEISA-19 linelist in the 1153-4775 cm^{-1} spectral range (in the HITRAN's type format [2]).

Supp-2: Results of the calculation of the {(0,1,1),(0,3,0)] energy levels. List of assignments for the $\nu_2+\nu_3-\nu_2$ hot band. List of assignments for the (0,1,1)-(0,1,0) hot band.

Supp-3: Results of the calculation of the {(1,0,2),(1,2,1)] energy levels, and list of assignments for the $\nu_1+2\nu_3-\nu_3$ hot band. List of assignments for the (1,0,2)-(0,0,1) hot band.

Supp-4: Partition function for $^{15}N^{16}O_2$.

Supp-5: Table TA1 and list of nine figures (A1-A9).

Table TA1 :

Comparison of the line positions and intensities in the 2814-2815 cm^{-1} spectral range of the FTS13 spectrum (see Fig. 10)

Fig A1 : Overview of the FTS3 spectrum (ν_3 band spectral region)

Fig A2:Overview of the $\nu_1+\nu_2$ band (FTS12).

Fig A3: Portion of the R branch of the $\nu_1+\nu_2$ band in the 2090 - 2093 cm^{-1} region (FTS12). We give some [N, K_a,K_c] (J=N±1/2) rotational assignments for the $\nu_1+\nu_2$ band. A comparison between the model provided by GEISA-19 and HITRAN2016-updated (or HITEMP) is given.

Fig. A4 : Portion of the R branch of the $\nu_2+\nu_3$ band in the 2365.2 cm^{-1} region (FTS23). In the bottom part of the figure, the quoted [N, K_a, K_c] (and eventually J) assignments are for the (0,1,1) upper sate energy levels. A comparison between the model provided by GEISA-19 and HITRAN2016-updated (or HITEMP) is given.

Fig. A5 : Portion of the P- branch of the $2\nu_2+\nu_3$ band near 3079.8 cm^{-1} (FTS223). In the upper part of the figure, the quoted [N, K_a, K_c] (and eventually J) assignments are for the (0,2,1) upper energy levels. The GEISA-19 and HITEMP (or HITRAN2016 -updated) linelists are compared.

Fig. A6: Portion of the R- branch of the $\nu_1+\nu_2+\nu_3$ band of NO_2 in the 3650 cm^{-1} region (FTS111 spectrum). Several N' assignments in the upper state are given for, [N,K_a = 0,K_c = N] = [N-1, 0, N-1] (triangles). This band is not considered in the HITEMP or HITRAN2016-updated databases.

Fig. A7 : Portion of the R- branch of the $2\nu_1+\nu_3$ band near 4155.2 cm^{-1} (FTS113). In the bottom part of the figure, the quoted [N, K_a, K_c] (and eventually J) assignments are for the (2,0,1) upper energy levels of the $2\nu_1+\nu_3$ band. Due to a local resonance the [23,3,21]-[24,0,24] transition of the dark $2\nu_1+2\nu_2$ band are observable on the spectrum. The GEISA-19 and HITEMP (or HITRAN2016-updated) linelists are compared.

Fig. A8 : Portion of the R- branch of the $3\nu_3$ band near 4774.8 cm^{-1} (FTS333). In the bottom part of the figure, the quoted [N, K_a, K_c] (and J, eventually) assignments are for the (0,0,3) upper energy levels of the $3\nu_3$ band. The GEISA-19 and HITEMP linelists are compared.

Fig. A9 : Overview of the FTS13 spectrum in the 2500-3000 cm^{-1} spectral region of the NO_2 absorption region. For NO_2, this spectral region corresponds to the $2\nu_1$ band and to the $\nu_1+\nu_3$ band and its associated hot bands. In this spectral region absoptions due the $\nu_1+\nu_{11}$ and $\nu_5+\nu_{11}$ bands of the N_2O_4 dimer are quite observable at 2630 and 2971 cm^{-1}, respectively. For NO_2, the comparison of the line by line model generated using the GEISA-19 and HITEMP databases are also presented. As noticed in Ref. [18] the $2\nu_1$ (B-type) band exibits an "anusual" intensity behaviour, with a very weak P- branch. In HITEMP, the line intensities of the $2\nu_1$ band are underestimated by a factor of about two, and the strange intensity pattern is not accounted for.

References

[1] N. Jacquinet-Husson, R. Armante, N.A. Scott, A. Chédin, L. Crépeau, C. Boutammine, A.Bouhdaoui, C. Crevoisier, V. Capelle, C. Boonne, N. Poulet-Crovisier, A. Barbe, D.C.Benner, V. Boudon, L.R. Brown, J. Buldyreva, A. Campargue, L.H. Coudert, V.M. Devi, M.J. Down, B.J. Drouin, A. Fayt, C. Fittschen, J.-M. Flaud, R.R. Gamache, J.J. Harrison, C. Hill C, Ø. Hodnebrog. S.M. Hu, D. Jacquemart, A. Jolly, E. Jiménez, N. Lavrentieva, A.W. Liu, L. Lodi, O.M. Lyulin, S.T. Massie, S. Mikhailenko, H.S.P. Müller, O.V. Naumenko, A. Nikitin, C.J. Nielsen, J. Orphal, V. Perevalov, A. Perrin, E. Polovtseva, A.Predoi-Cross, M. Rotger, A.A. Ruth, Y. Shanshan, K. Sung, S. Tashkun, J. Tennyson, V.G. Tyuterev, J. Vander Auwera, B. Voronin, and A. Makie. J. Mol. Spectrosc. 327 (2016) 31-72.

[2] I.E. Gordon, Rothman LS, Hill C, Kochanov RV, Tana Y, Bernath PF, Birk M, Boudon V, Campargue A, Chance KV, B.J. Drouin, J.-M. Flaud, R.R. Gamache, J.T.Hodges, D. Jacquemart, V.I. Perevalov, A. Perrin, Shine KP, Smith MA, Tennyson J, Toon GC, Tran H, Tyuterev VG, A. Barbe, A.G. Császár, V.M. Devi, T. Furtenbacher, J.J. Harrison, J.M. Hartmann, A. Jolly, T.J. Johnson, T. Karman, I. Kleiner, A.A. Kyuberis, J. Loos, O.M. Lyulin, S.T. Massie, S.N. Mikhailenko, N. Moazzen-Ahmadi, H. Müller, O.V. Naumenko, A.V. Nikitin, O.L. Polyansky, M. Rey, M. Rotger, S.W. Sharpe, K. Sung E. Starikova, S.A.Tashkun, J. Vander Auwera, G. Wagner, J. Wilzewski, P. Wcisło, S. Yuh, E.J. Zak. J. Quant. Spectrosc. Radiat. Transf. **203**, (2017) 3-69.

[3] R.J. Hargreaves, I. E. Gordon, L. S. Rothman, S. A. Tashkun, V. I. Perevalov, A. A. Lukashevskaya, S. N. Yurchenko, J. Tennyson, and H. S.P. Müller. J. Quant. Spectrosc. Radiat. Transf**.** 232 (2019) 35-53.

[4] A.A. Lukashevskaya, O.M. Lyulin, A. Perrin, and V. I. Perevalov, Atmospheric and Oceanic Optics, 28 (2015) 216-231.

[5] A.A. Lukashevskaya, N.N. Lavrentieva, A.C. Dudaryonok, and V.I. Perevalov. J. Quant. Spectrosc. Radiat. Transf. 184 (2016) 205-217 ; *ibid.* 202 (2017) 37-37.

[6] High-resolution transmission molecular absorption database (HITRAN). [https://hitran.org/]

[7] A.A.Lukashevskaya, O.V.Naumenko, S.Kassi, A.Campargue. J. Quant. Spectrosc. Radiat. Transfer. 338 (2017) 91-96.

[8] A.A.Lukashevskaya, S.Kassi, A.Campargue, V.I.Perevalov. J. Quant. Spectrosc. Radiat. Transfer. 202 (2017) 302-307.

[9] A.A.Lukashevskaya, S.Kassi, A.Campargue, V.I.Perevalov. J. Quant. Spectrosc. Radiat. Transfer. 200 (2017) 17-24.

[10] A.A.Lukashevskaya, D.Mondelain, A.Campargue, V.I.Perevalov. J. Quant. Spectrosc. Radiat. Transfer. 219 (2018) 393-398.

[11] O.V.Naumenko, A.A.Lukashevskaya, S.Kassi, S.Béguier, A.Campargue. J. Quant. Spectrosc. Radiat. Transfer. 232 (2019) 146-151.

[12] A.Perrin, S.Kassi and A.Campargue. J. Quant. Spectrosc. Radiat. Transf. 111, (2010) 2246–2255.

[13] D. Mondelain, A.Perrin, S. Kassi, A. Campargue.. J. Quant. Spectrosc. Radiat. Transf. 113 (2012) 1058-1065.

[14] A.A. Lukashevskaya, O.V. Naumenko, A. Perrin, D. Mondelain, S. Kassi and A. Campargue, , J. Quant. Spectrosc. Rad. Trans., **130**, (2013) 249-259.

[15] A.A. Lukashevskaya, O.V. Naumenko, D. Mondelain, S.Kassi, J. Quant. Spectrosc. Radiat. Transf. 177 (2016) 225-233.

[16] A. Perrin, G. Toon, J. Orphal. J. Quant. Spectrosc. Radiat. Transfer. 154 (2015) 91–97

[17] F. Gueye, F. Kwabia Tchana, X. Landsheere, and A. Perrin. J. Quant. Spectrosc. Radiat. Transf. 138 (2014) 60-69.

[18] A. Perrin, L. Manceron , and F. Kwabia Tchana (2020). Mol. Phys. 118 (2020) DOI: 10.1080/00268976.2019.1711235.

[19] A. Perrin, J.-M. Flaud, C. Camy-Peyret, B. Carli, and M. Carlotti. Mol. Phys. 63 (1988) 791-910.

[20] A. Perrin, C. Camy-Peyret, J.-M. Flaud, and J. Kauppinen. J. Mol. Spectrosc. 130 (1988) 168-182.

[21] J.K.G. Watson, in: J.R. Durig (Ed.), Vibrational Spectra and Structure, vol. 6, Elsevier, Amsterdam, 6 (1997) 1–89.

[22] I. C. Bowater, J. M. Brown, and A. Carrington, F.R.S. Proc. B. Soc. Lond. A. 333 (1973) 265-288.

[23] A. Perrin, J.-M. Flaud, C. Camy-Peyret, A.-M.Vasserot, G. Guelachvili, A. Goldman, F.J. Murcray, and R.D.Blatherwick. J. Mol. Spectrosc. 154 (1992) 391-406.

[24] A. Perrin, M. Ndao, and L. Manceron. J. Quant. Spectrosc. Radiat. Transf. 200 (2017) 12-16.

[25] De Bievre P, Holden NE, Barnes IL. J. Phys. Chem. Ref. Data 13 (1984) 809–891.

[26] J.-Y. Mandin, V. Dana, A. Perrin, J.-M. Flaud, C. Camy-Peyret, L. Régalia, and A. Barbe, J. Mol. Spectrosc. 181 (1997) 379-388.

[27] D. C. Benner, T.A. Blake, L.R. Brown, V. Malathy Devi, M.A.H. Smith, and R.A. Toth. J. Mol. Spectrosc. 228 (2004) 593-619.

[28] J.M.Hartmann (private communication).

[29] A. Perrin, J.-M. Flaud, C. Camy-Peyret, D. Hurtmans, and M. Herman and G.Guelachvili. J. Mol. Spectrosc. 168 (1994) 54-66.

[30] S. Reymond-Laruinaz, M. Faye, V. Boudon, D. Doizi, and L. Manceron, , J. Mol. Spectrosc. 336 (2017) 29-35.

[31] M. Faye, M. Bordessoule, B. Kanouté, J.-B. Brubach, P. Roy, L.Manceron, Rev. Sci. Inst. 87, 063119 (2016).

[32] K. Schofield, Evaluated chemical kinetic rate constants for variuous gas phase reactions. J. Phys. Chem. Ref. Data. 2 (1973) 25-84.

[33] A. Perrin, J.-M. Flaud, C. Camy-Peyret, A. Goldman, J.F.Murcray, R.D. Blatherwick, and C.P. Rinsland. J. Mol. Spectrosc. 160, 456–463 (1993).

[34] A. Perrin, J.-M. Flaud, C. Camy-Peyret, D. Hurtmans, D.Hurtmans, and M. Herman. J. Mol. Spectrosc. 177 (1996) 58-65.

[35] T.M. Stephen, A. Goldman, A. Perrin, J.-M. Flaud, F. Keller, and C.P. Rinsland. J. Mol. Spectrosc. 201 (2000) 134-142.

[36] S.Sharpe, T.Johnson, R. Sams, P.Chu, G.Rhoderick, P.Johnson, Appl. Spectrosc. 58 (2004) 1452– 1461.

[37] N. Semmoud-Monnanteuil, J.-M. Colmont, A. Perrin, J.-M. Flaud, and C. Camy-Peyret, J. Mol. Spectrosc. 134 (1989) 176 -182.

[38] C. Camy-Peyret, J.-M. Flaud, A. Perrin, and K. Narahari-Rao, J. Mol. Spectrosc. 95 (1982) 72-79.

[39] A. Perrin, J. -M. Flaud, A. Goldman, C. Camy-Peyret, W.J. Lafferty, Ph. Arcas, and C.P. Rinsland, J. Quant. Spectrosc. Radiat. Transfer. 60 (1998) 839- 850.

[40] A.Perrin, J.-M.Flaud, C.Camy-Peyret, Infrared Phys. 22 (1982) 343-348.

[41] A.Delon, and R.Jost, J. Chem. Phys. 95 (1991) 5686-5700. https://doi.org/10.1063/1.461617

[42] A.Perrin, J.-M.Flaud, C.Camy-Peyret, A. N'Gom, R. M'Biake, H. Gbaguidi, and G. Guelachvili, J. Mol. Spectrosc. 171 (1995) 354-357.

[43] S. Miljanic, A. Perrin, and J. Orphal, J. Mol. Spectrosc. 242 (2007) 176–181.

List of figures

Fig. 1 : Portion of the P- branch of the strong ν_3 band of NO_2 near 1557 cm^{-1} (FTS3 bis). The prediction provided by the GEISA-19 , HITEMP and HITRAN2016-updated linelists are compared. Transitions belonging to the P branch $\nu_2+\nu_3-\nu_2$ hot band are identified by their upper level (0,1,1) in the upper part of the figure. The corresponding predictions by HITEMP or HITRAN2016-updated are quoted. Note that both HITRAN2016-updated and GEISA-19 include the list for the ν_3 band of $^{15}N^{16}O_2$, while this is not the case for HITEMP. The "$" indicates a strong water line.

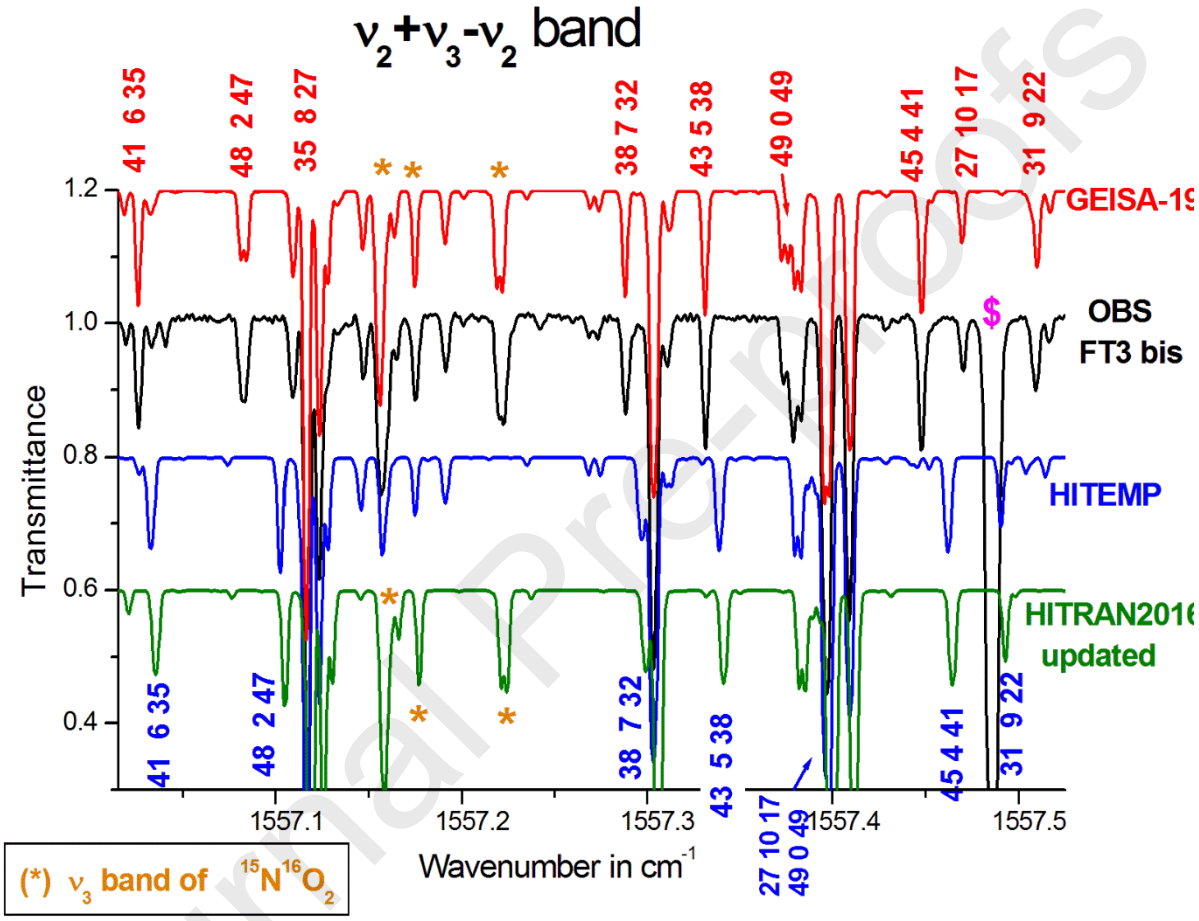

Fig. 2: Portion of the P- branch of the ν_3 band in the 1555.7 cm^{-1} spectral range (FTS3 bis). The GEISA-19, HITEMP, and HITRAN2016-updated linelists are compared. Transitions belonging to the P branch $\nu_1+\nu_3-\nu_1$ hot band are identified by their upper level (1,0,1) rotational quantum numbers on the GEISA-19 trace. The predictions by HITEMP are also quoted. Note that both HITRAN2016-updated and GEISA-19 include the list for the ν_3 band of $^{15}N^{16}O_2$, while this is not the case for HITEMP.

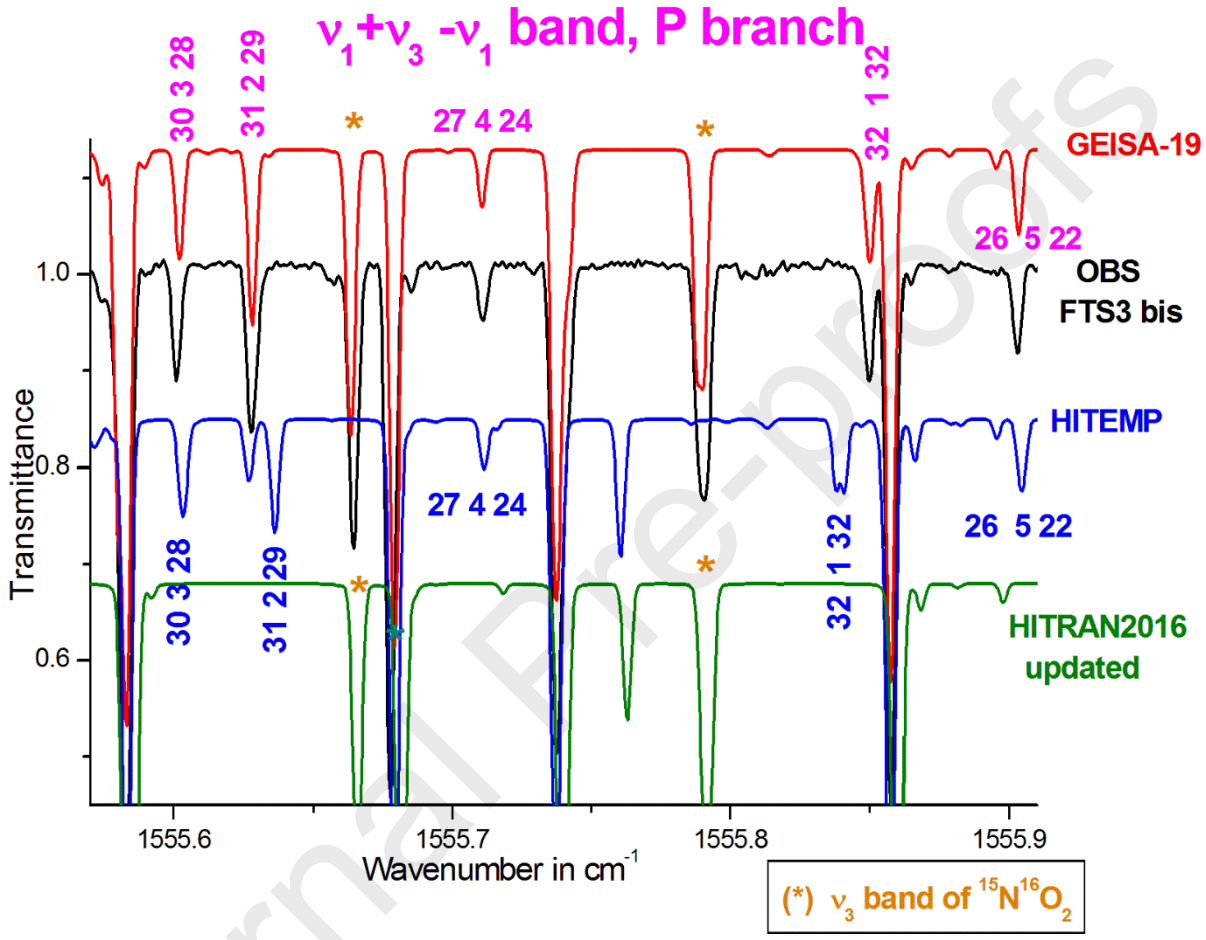

Fig. 3: Portions of the P- branch of the ν_3 band in the 1561- 1568 cm^{-1} spectral range. Two transitions belonging to the P branch $2\nu_2+\nu_3-2\nu_2$ and $\nu_1+\nu_3-\nu_1$ hot bands are identified. The GEISA-19 and HITEMP linelists are compared. . Note that both HITRAN2016-updated and GEISA-19 include the list for the ν_3 band of $^{15}N^{16}O_2$, while this is not the case for HITEMP.

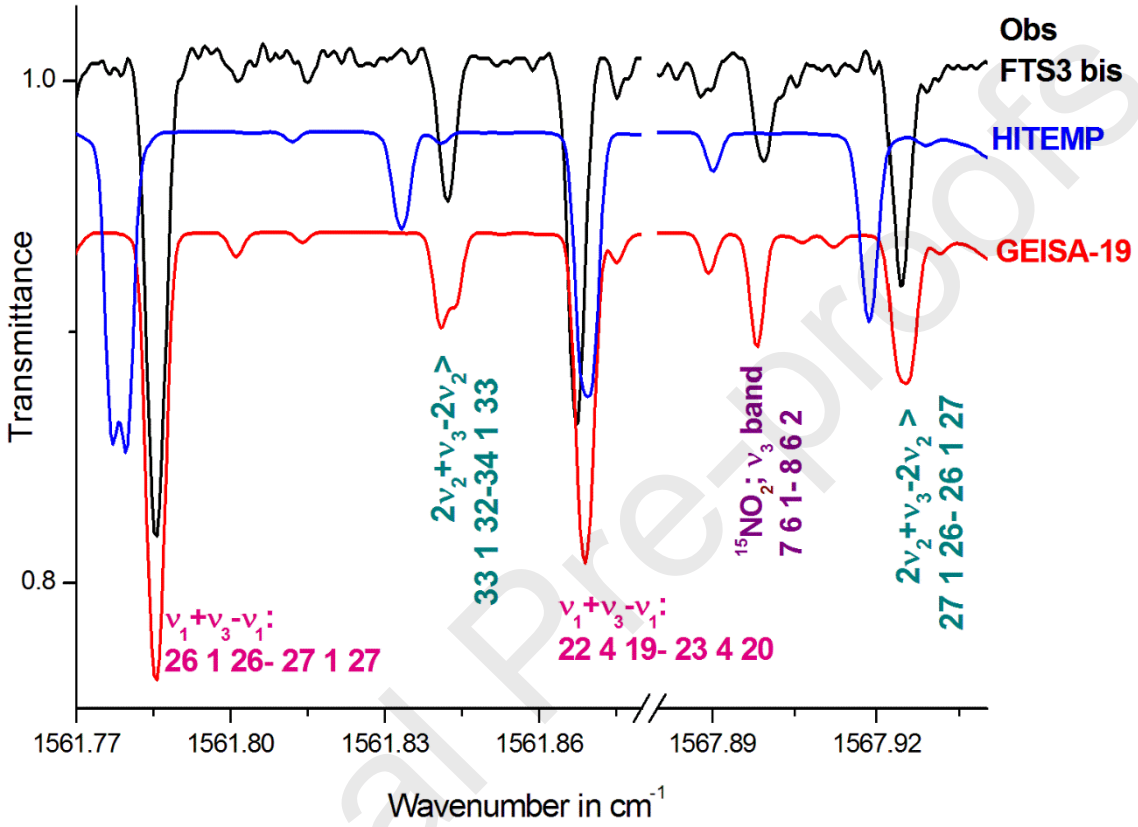

Fig. 4: Portions of the P- branch of the ν_3 band in the 1572- 1575 cm-1 spectral range (FTS3 spectrum). We identify transitions belonging to the P branches of the $\nu_2+\nu_3-\nu_2$, $2\nu_3-\nu_3$ and $2\nu_2+\nu_3-2\nu_2$ hot bands. The GEISA-19 and HITEMP linelists are compared.

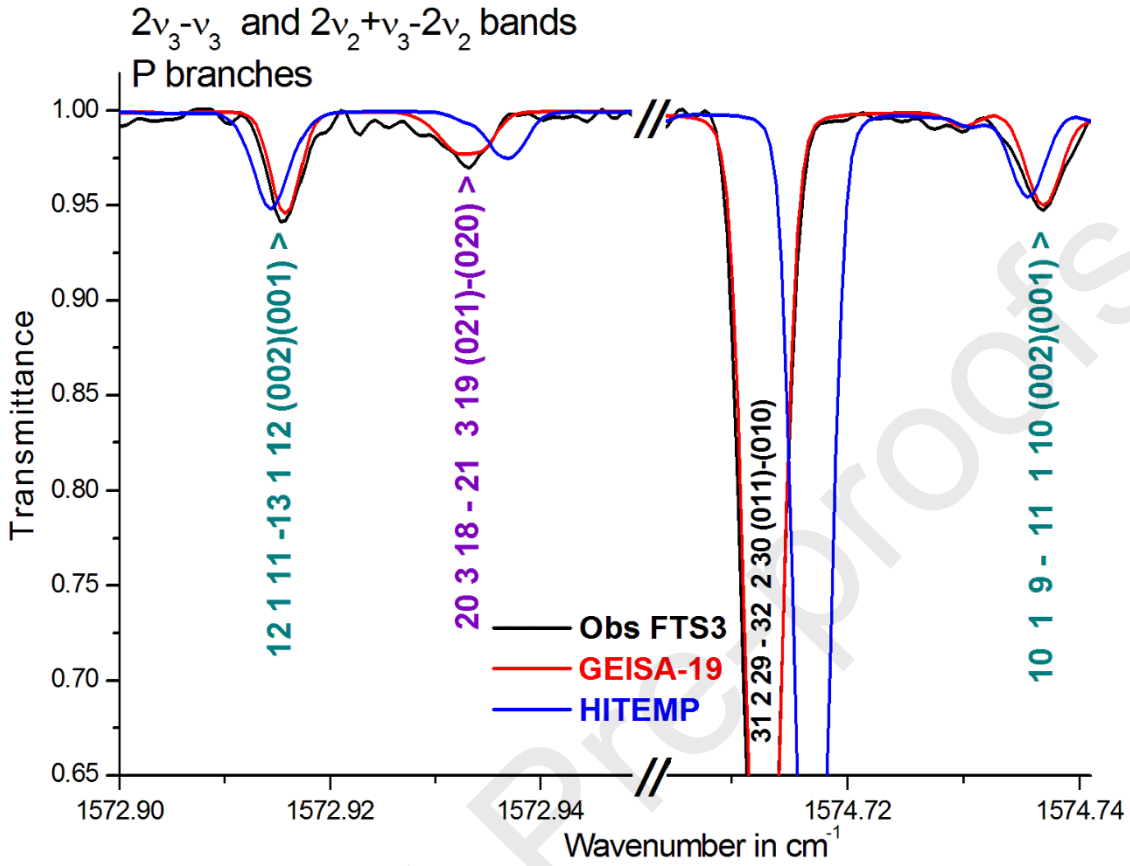

Fig 5: Portion of the P- branch of the ν_3 band in the 1559.1 cm^{-1} spectral range (FTS3 spectrum). In this region, lines from hot bands together with those the ν_3 of $^{15}N^{16}O_2$ are observable. The models provided by GEISA-19, HITRAN2016-updated and HITEMP are compared. Note that both HITRAN2016-updated and GEISA-19 include the list for the ν_3 band of $^{15}N^{16}O_2$, while this is not the case for HITEMP.

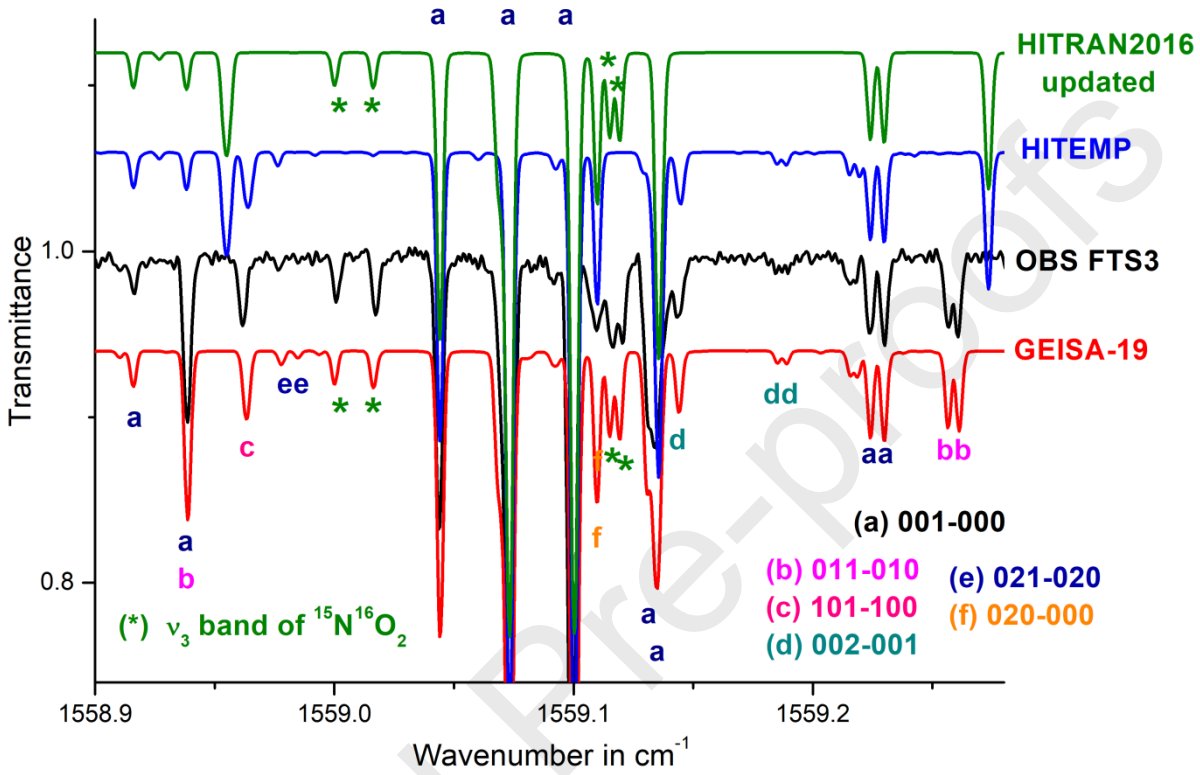

Fig. 6: Portion of the P- branch of the $\nu_1+\nu_3$ band of NO_2 near 2838.8 cm^{-1} (FTS13). The GEISA-19 and HITEMP linelists are compared. On the GEISA-19 trace, lines belonging to the $\nu_1+\nu_2+\nu_3-\nu_2$ hot band are indicated by their [N, K_a, K_c] (and J, eventually) assignments are for the (1,1,1) upper energy levels of the $\nu_1+\nu_2+\nu_3-\nu_2$ band. The corresponding predictions in HITEMP are also given.

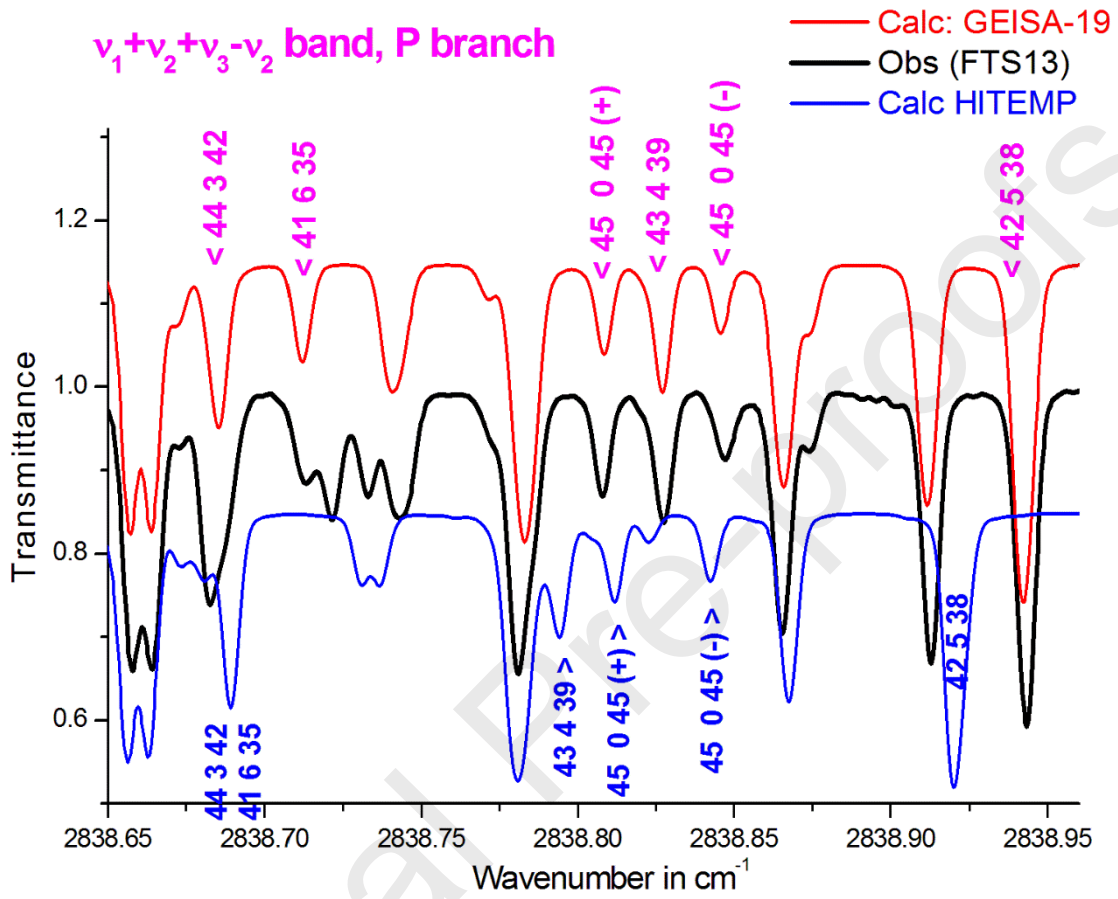

Fig 7: Portion of the P- branch of the $\nu_1+\nu_3$ band in the 2821.6 cm^{-1} spectral range (FTS13 spectrum). The calculated spectra using GEISA-19 and HITEMP are compared to the observation. Lines from the $\nu_1+2\nu_3-\nu_3$ hot band are indicated by their rotational quantum assignments in the (1,0,2) upper state are given on the GEISA-20 trace. The coresponding predictions by HITEMP are also quoted.

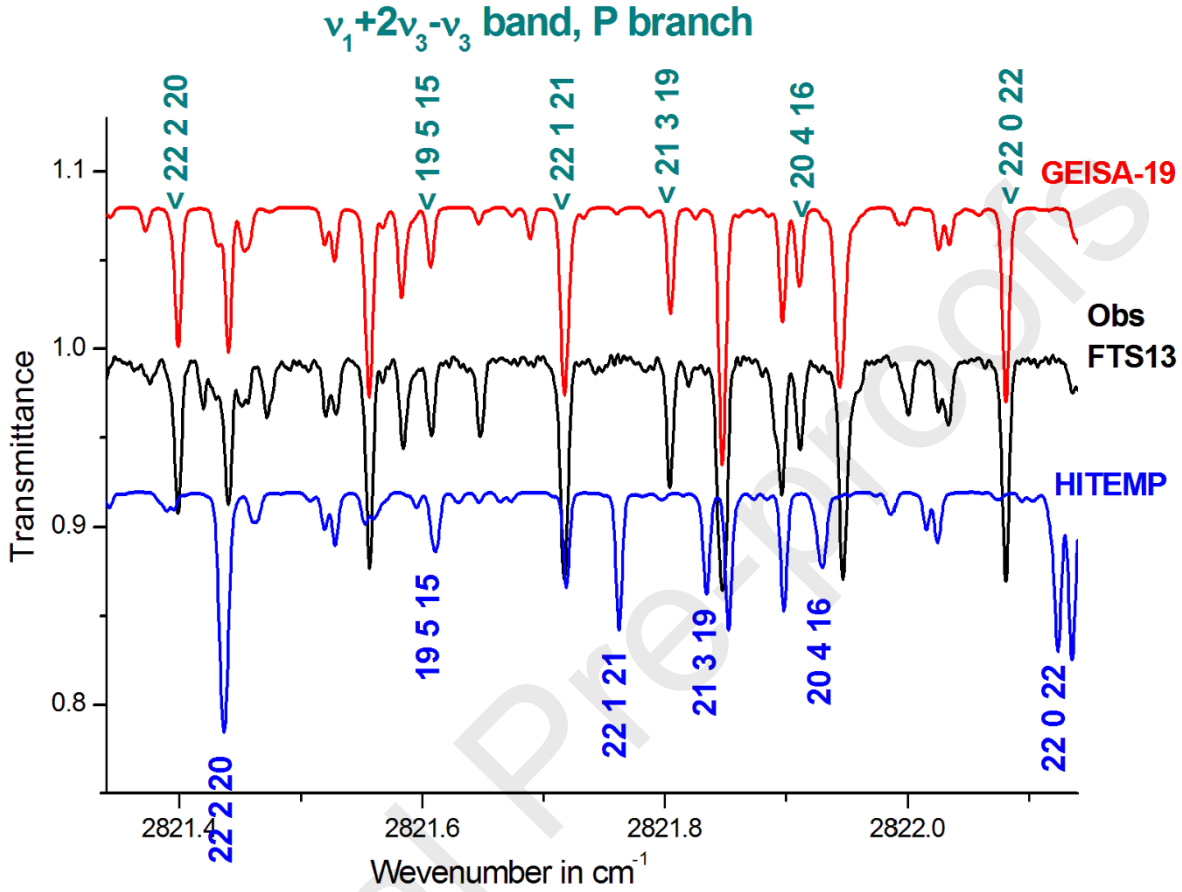

Fig 8: Portion of the P- branch of the $\nu_1+\nu_3$ band in the 2834.8 cm^{-1} spectral range (FTS13 spectrum). The model provided by GEISA-19 and HITEMP are compared. Transitions belonging to the P branch $2\nu_1+\nu_3-\nu_1$ hot band are are identified by their rotational quantum numbers in the (2,0,1) upper state in GEISA-19. The corresponding predictions by HITEMP are quoted therein.

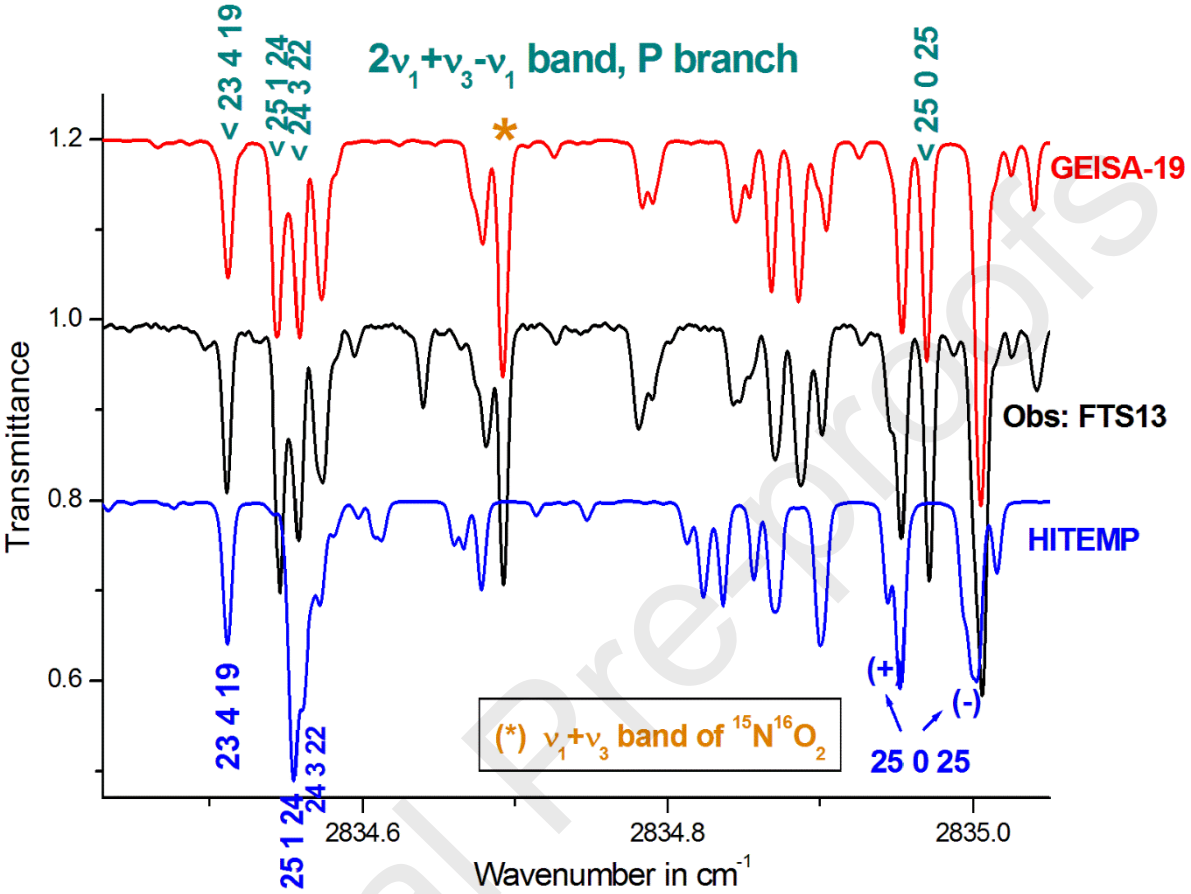

Fig 9: Portion of the P- branch of the $\nu_1+\nu_3$ band in the 2820 cm^{-1} spectral range (FTS13 spectrum). In this region, lines from the $\nu_1+\nu_3$ band of $^{15}N^{16}O_2$ are also observable, together with numerous lines from the hot bands from the main species. The model of the observed spectrum performed by GEISA-19, HITRAN2016-updated and HITEMP are compared. In this region, HITRAN2016-updated includes only lines from the $\nu_1+\nu_3$ band of of $^{14}N^{16}O_2$.

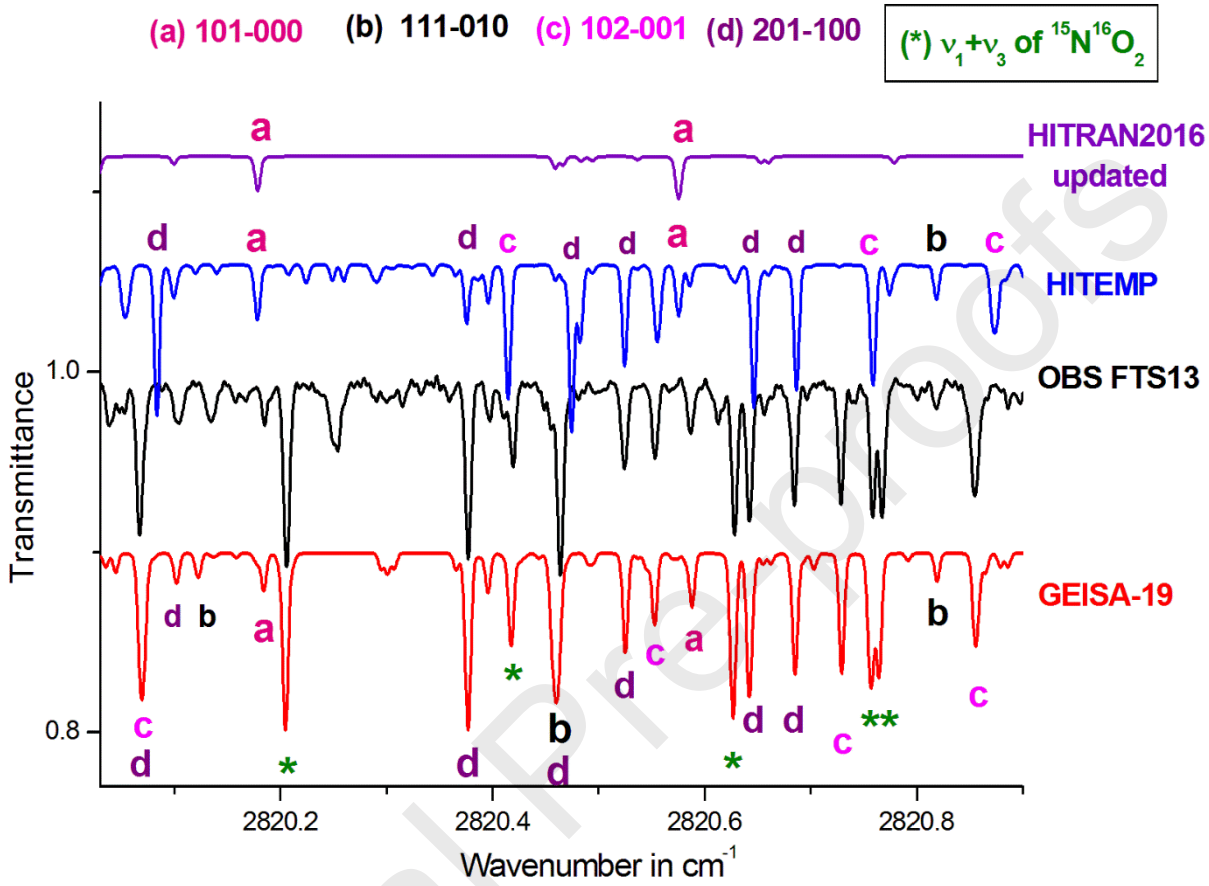

Fig. 10 : Portion of the P branch of $\nu_1+\nu_3$ band and of the R branch of the the $2\nu_1$ band in the 2814.4 cm^{-1} regions (FTS13). The upper and lower traces compare the observed spectrum to line by line models performed using the HITEMP and GEISA-19 linelists, respectively. On the "GEISA-19" trace, the assignments for two (split) doublets of the $2\nu_1$ band are also given, and compared to their corresponding (unsplit doublets) predictions in HITEMP. Lines from the P branches of the $2\nu_1+\nu_3-\nu_1$ and the $\nu_1+2\nu_3-\nu_3$ hot bands of $^{14}N^{16}O_2$ and of the $\nu_1+\nu_3$ band of the $^{15}N^{16}O_2$ isotopic species species are also indicated. More detailed assignments are provided in Table TA1 of "Supp-5" of the Supplementary data.

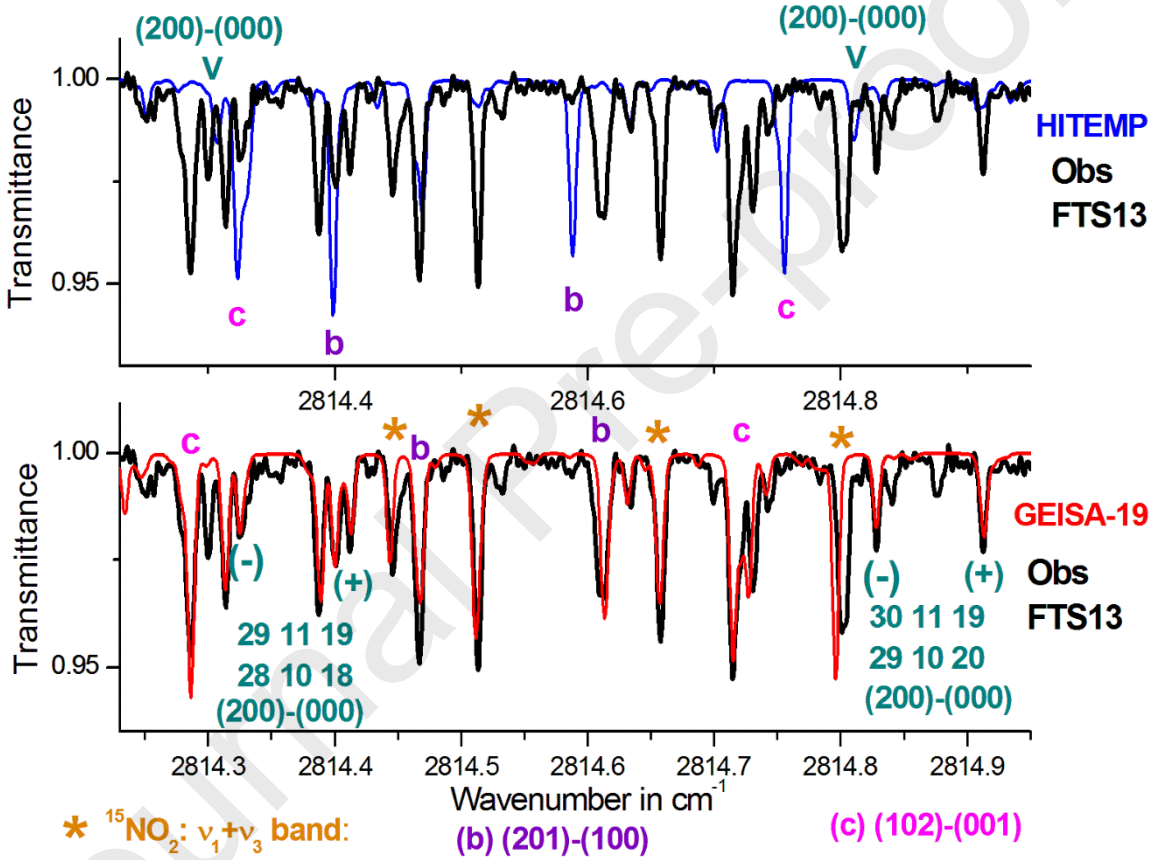

Fig 11: The PNNL cross sections for NO_2 (NO2_25T). Comparison with the computed cross sections using the GEISA-19 and HITEMP databases.

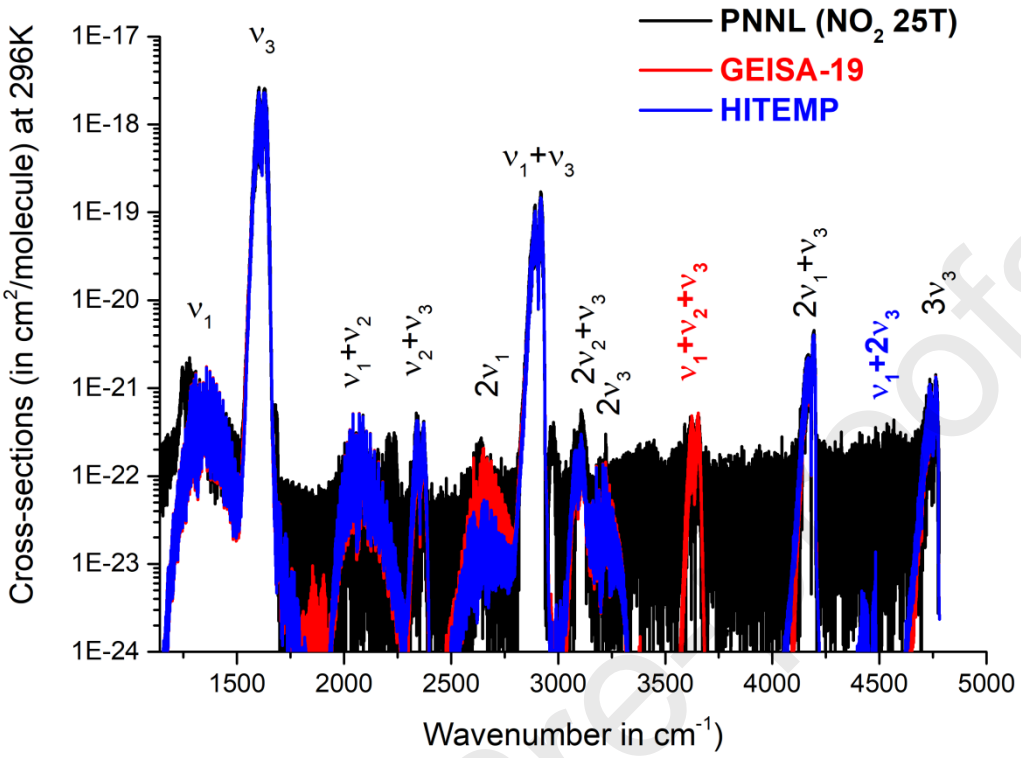

Table 1
Hamiltonian matrix

	(v_1', v_2', v_3')	(v_1, v_2, v_3)
(v_1', v_2', v_3')	W+SR	C
(v_1, v_2, v_3)	C	W+SR

With $(v_1', v_2', v_3') = (0,3,0)$ and $(v_1, v_2, v_3) = (0,1,1)$;
or $(v_1', v_2', v_3') = (1,0,2)$ and $(v_1, v_2, v_3) = (1,2,1)$.

Example of a "W+SR" Watson "W" and spin-rotational "SR" v-diagonal block:

		(v_1, v_2, v_3)	
		N = J-1/2	**N = J+1/2**
(v_1, v_2, v_3)	**N = J-1/2**	$W_{vv} + SR_{vv}$	SR_{vv}
	N = J+1/2	SR_{vv}	$W_{vv} + SR_{vv}$

Example of a Coriolis "C" vibrational off diagonal block:

		(v_1, v_2, v_3)	
		N = J-1/2	**N = J+1/2**
(v_1', v_2', v_3')	**N = J-1/2**	$C_{v'v}$	
	N = J+1/2		$C_{v'v}$

W_{vv}: Watson's A-type I^r representation Hamiltonian.

$$W_{vv} = E_v + \left[A^v - \tfrac{1}{2}\left(B^v + C^v\right)\right]N_z^2 + \tfrac{1}{2}\left(B^v + C^v\right)\mathbf{N}^2 + \tfrac{1}{2}\left(B^v - C^v\right)N_{xy}^2$$
$$- \Delta_K^v N_z^4 - \Delta_{JK}^v N_z^2\mathbf{N}^2 - \Delta_J^v\left(\mathbf{N}^2\right)^2 - \delta_K^v\left\{N_z^2, N_{xy}^2\right\} - 2\delta_J^v N_{xy}^2\mathbf{N}^2$$
$$+ H_K^v N_z^6 + H_{KJ}^v N_z^4\mathbf{N}^2 + H_{JK}^v N_z^2\left(\mathbf{N}^2\right)^2 + H_J^v\left(\mathbf{N}^2\right)^3$$
$$+ h_K^v\left\{N_z^4, N_{xy}^2\right\} + h_{KJ}^v\left\{N_z^2, N_{xy}^2\right\}\mathbf{N}^2 + 2h_J^v N_{xy}^2\left(\mathbf{N}^2\right)^2 + \ldots$$

SR_{vv} : Electron-spin rotation interactions.

$$SR_{vv} = \varepsilon_{aa}^v S_a N_a + \varepsilon_{bb}^v S_b N_b + \varepsilon_{cc}^v S_c N_c +$$

$$\Delta_N^{vS} N^2 (N.S) + \frac{1}{2}\Delta_{NK}^{vS}\left\{N^2 N_z S_z + S_z N_z N^2\right\} + \Delta_{KN}^{vS}(N.S)$$
$$+ \Delta_K^{vS} N_z^3 S_z + \delta_N^{vS}\left(N_+^2 + N_-^2\right)(N.S) + \frac{1}{2}\delta_K^{vS}\left\{\left(N_+^2 + N_-^2\right)N_z S_z + N_z S_z\left(N_+^2 + N_-^2\right)\right\}$$

$C_{v'v}$: Coriolis-type interactions (for $|\Delta v_3|$= odd):

$$C_{v'v}^{C} = h_{v'v}^{1C}\, i\, N_y + h_{v'v}^{2C}\left(N_-^3 - N_+^3\right) + \mathbf{...}$$

with: $N_{xy}^2 = N_x^2 - N_y^2$, $N_\pm = N_x \mp i N_y$, and $\{X, Y\} = XY + YX$

cc: complex conjugate

Table 2

FTS spectrum	Laboratory	Main band	Spectral range in cm^{-1}	NO_2 pressure in hPa	Path lenth in m.	Ref.
FTS12	AILES on SOLEIL	$\nu_1+\nu_2$	1958-2289	≈ 4.9	10.88	This work
FTS3	AILES on SOLEIL	ν_3	1540-1665	0.2	2.72	This work
FTS3bis	AILES on SOLEIL	ν_3	1540-1665	0.62	2.72	This work
FTS13	AILES on SOLEIL	$2\nu_1$ and $\nu_1+\nu_3$	2520-3000	5.1	10.88	Ref. [18]
FTS23	ULB-Brussels	$\nu_2+\nu_3$	2270-2400	2.90	48.8	Ref. [29]
FTS33	ULB-Brussels	$2\nu_2+\nu_3$, $4\nu_2$, and $2\nu_3$	3000-3400	2.93	40.8	Ref. [34]
FTS123	University Paris Est	$\nu_1+\nu_2+\nu_3$	3578-3680	~3	41.6	Ref. [17]
FTS113	University of Denver	$2\nu_1+\nu_3$	4125-4210	???$	7.2	Ref.[35]
FTS333	University of Denver	$3\nu_3$	4680-4780	???$	7.2	Ref.[35]

All measurements were done at room temperature (~296K).

$ In Ref. [35] the partial pressure of the NO2 monomer was estimated at 10 hPa. This value may be incorrect (see text).

Table 3
Vibrational energies, spin-rotational and rotational constants:

	(000)[#]	**(0,3,0)**	**(0,1,1)**
E_v		2246.04 [a]	2355.14980(8)
A	8.00235469	9.2178873(640)	8.1261153(290)
B	0.433706798	0.433080(130)	0.430878518(290)
C	0.410442540	0.407802(140)	0.406866093(170)
Δ_K	0.26878757×10^{-2}	#	$0.3216229(600)\times10^{-2}$
Δ_{KN}	-0.196822×10^{-4}	#	$-0.2457511(860)\times10^{-4}$
Δ_N	0.2992447×10^{-6}	#	$0.306505(110)\times10^{-6}$
δ_K	0.40547×10^{-5}	#	$0.57572(420)\times10^{-5}$
δ_N	0.3192774×10^{-7}	#	$0.335862(400)\times10^{-7}$
H_K	0.303157×10^{-5}	#	$0.428664(940)\times10^{-5}$
H_{KN}	-0.270439×10^{-7}	#	$-0.24547(270)\times10^{-7}$
H_N	0.2866×10^{-12}	#	$0.5250(220)\times10^{-12}$
h_K	0.29297×10^{-7}	#	$0.46349(580)\times10^{-7}$
L_K	-0.51104×10^{-8}	#	$-0.72675(450)\times10^{-8}$
L_{KKN}	0.35117×10^{-10}	#	$1.8141(240)\times10^{-10}$
ε_{aa}^{v}	0.180353006	#	0.1886686(710)
ε_{bb}^{v}	0.257833×10^{-3}	#	$0.25761(510)\times10^{-3}$
ε_{cc}^{v}	-0.3178107×10^{-2}	#	$-0.32570(490)\times10^{-2}$
Δ_K^{vS}	-0.17606×10^{-3}	#	$-0.20700(130)\times10^{-3}$

Vibrational energies, spin-rotational and rotational constants:

	(1,0,2)	**(1,2,1)**
E_v	4460.8648(2)	4369.10 [a]
A	7.62253802(380)	8.1261153(290)
B	0.42593600(170)	0.430878518(290)
C	0.4020917(150)	0.406866093(170)
Δ_K	$0.252081(180)\times10^{-2}$	#
Δ_{KN}	$-0.251017(260)\times10^{-4}$	#
Δ_N	$0.309119(520)\times10^{-6}$	#
δ_K	$0.3879(430)\times10^{-5}$	#
δ_N	$0.3245(460)\times10^{-7}$	#
H_K	$0.29843(210)\times10^{-5}$	#
H_{KN}	$-0.2042(340)\times10^{-8}$	#
H_N	#	#
h_K	#	#
L_K	#	#
L_{KKN}	#	#
ε^v_{aa}	0.165066(270)	#
ε^v_{bb}	$0.2528(240)\times10^{-3}$	#
ε^v_{cc}	$-0.32199(230)\times10^{-2}$	#
Δ_K^{vS}	#	#

Higher order spin-rotational and rotational constants for all states :

Rotational constants[#]		**Spin-rotational constants[#]**	
H_{NK}	0.2995×10^{-10}	$\Delta_{KN}^{vS}+\Delta_{NK}^{vS}$	0.6005×10^{-6}
h_{KN}	-0.3637×10^{-10}	Δ_N^{vS}	0.6322×10^{-9}
h_N	0.1057×10^{-12}	Δ_{NK}^{vS}	0.1678×10^{-5}

L_{KN}	0.12158×10^{-12}	δ_K^{vS}	0.3769×10^{-6}
P_K	0.867×10^{-11}	δ_N^{vS}	0.244×10^{-9}
Q_K	-0.839×10^{-14}	H_K^S	0.29673×10^{-6}
		L_K^S	-0.3569×10^{-9}

Coriolis resonances

Operator	**(0,3,0)-(0,1,1)**	**(2,1,0)-(2,0,1)**
$i N_y$	0.046100(350)	0.0517441(430)

Note: The results are in cm^{-1} and the quoted errors correspond to one standard deviation. The spin–rotational constants, the higher order rotational constants together with constants marked with # were held fixed to the ground state values [37]. [a] From Ref. [41].

Table 4
Description of the GEISA-19 database (1153- 4775.4 cm^{-1})
The $^{14}N^{16}O_2$ linelist:

									Calculation		Observation	
V'	V''	Nb	Centre	S_min	S_max	Band Int	Int_{Min}	Int_{Max}	N Max	K_a range	N Max	K_a range
101	001	966	1289.89	1224.94	1607.29	0.185E-22	0.10E-25	0.59E-25	52	0-8	75	0-14
100	000	8145	1319.79	1153.01	1664.24	0.721E-19	0.10E-24	0.17E-21	79	0-16	56	0-15
101	020	2	1408.40	1508.14	1615.42	0.204E-25	0.10E-25	0.10E-25	65	8	60	1-6
220	200	5	1473.24	1530.94	1582.85	0.285E-24	0.14E-25	0.11E-24	44	2-3	0	0
021	001	239	1475.63	1533.53	1621.31	0.450E-21	0.11E-24	0.49E-23	53	4-8	49	0-6
130	110	78	1483.98	1533.70	1605.43	0.132E-23	0.10E-25	0.73E-25	43	3-5	0	0
120	100	520	1485.81	1455.08	1652.23	0.230E-22	0.10E-25	0.16E-24	65	0-7	0	0
040	020	256	1494.66	1545.26	1631.78	0.140E-20	0.10E-24	0.20E-22	52	3-5	41	K_a=5
030	010	1927	1496.39	1429.25	1690.68	0.761E-21	0.20E-25	0.16E-22	71	0-8	0	0
020	000	4426	1498.34	1369.96	1800.30	0.645E-19	0.10E-24	0.61E-21	82	0-14	62	0-6
201	200	1659	1552.60	1503.90	1586.05	0.150E-21	0.10E-25	0.36E-24	51	0-10	55	0-11
003	002	850	1552.77	1516.38	1581.14	0.244E-22	0.10E-25	0.66E-25	40	0-8	60	0-8
102	101	1350	1554.12	1510.73	1586.95	0.765E-22	0.10E-25	0.18E-24	47	0-9	45	0-8
111	110	3073	1574.72	1509.97	1614.74	0.238E-20	0.10E-25	0.56E-23	61	0-12	55	0-10
002	001	3147	1584.59	1517.86	1626.60	0.432E-19	0.10E-24	0.99E-22	65	0-10	60	0-8

101	100	4383	1586.95	1504.16	1667.57	0.909E-19	0.10E-25	0.21E-21	65	0-10	56	0-10
021	020	3032	1594.14	1526.69	1635.95	0.351E-19	0.10E-24	0.88E-22	65	0-10	49	0-6
011	010	6947	1605.50	1505.60	1752.36	0.145E-17	0.20E-25	0.34E-20	71	0-13	63	0-10
001	000	10856	1616.85	1429.63	1835.38	0.569E-16	0.10E-24	0.13E-18	90	0-18	81	0-15
002	020	243	1703.10	1525.53	1616.92	0.314E-21	0.10E-24	0.36E-23	55	4-5	55	4-5
002	100	880	1881.65	1754.08	1953.09	0.186E-21	0.10E-24	0.72E-24	53	4-5	49	0-6
110	000	7593	2063.12	1921.88	2346.16	0.165E-19	0.10E-25	0.41E-22	65	0-14	61	0-10
011	000	2551	2355.15	2289.98	2395.03	0.850E-20	0.50E-25	0.23E-22	62	0-10	63	0-10
200	000	5982	2627.34	2457.95	2921.80	0.839E-20	0.50E-25	0.23E-22	71	0-16	62	0-12
130	010	293	2797.45	2826.76	2924.89	0.671E-22	0.51E-25	0.23E-23	47	3-5	0	0
120	000	1531	2805.60	2740.02	3023.06	0.853E-21	0.50E-25	0.53E-23	77	0-9	61	3-5
102	001	1836	2844.01	2787.39	2872.69	0.217E-20	0.10E-24	0.51E-23	53	0-10	45	0-8
201	100	3245	2860.14	2790.47	2888.91	0.923E-20	0.50E-26	0.22E-22	52	0-10	55	0-11
111	010	3904	2888.19	2811.08	2919.85	0.734E-19	0.51E-25	0.17E-21	61	0-12	55	0-12
101	000	8731	2906.74	2688.75	3148.79	0.287E-17	0.50E-25	0.66E-20	80	0-16	75	0-14
040	000	194	2993.00	3040.81	3133.67	0.257E-21	0.11E-24	0.37E-23	49	3-5	41	K_a=5
021	000	2512	3092.48	3032.58	3283.84	0.650E-20	0.10E-24	0.15E-22	58	0-12	49	6
002	000	3597	3201.44	3019.48	3322.09	0.377E-20	0.10E-24	0.14E-22	65	0-10	60	0-8
210	000	1018	3364.57	3291.70	3658.07	0.215E-22	0.10E-25	0.15E-24	52	0-9	0	0
130	000	275	3547.10	3581.21	3678.91	0.110E-22	0.10E-25	0.36E-24	46	3-5	0	0
111	000	3999	3637.84	3563.65	3690.60	0.123E-19	0.10E-25	0.28E-22	61	0-15	55	0-12
220	000	333	4100.58	4100.56	4207.21	0.191E-21	0.50E-25	0.58E-22	63	2-7	N=23	3
201	000	4234	4179.94	4087.83	4230.50	0.790E-19	0.50E-25	0.18E-21	66	0-13	55	0-11
022	000	133	4656.34	4702.20	4768.40	0.145E-22	0.50E-25	0.18E-24	41	5-6	0	0
003	000	3647	4754.21	4624.75	4775.31	0.304E-19	0.50E-25	0.70E-22	66	0-12	57	0-10

The $^{15}N^{16}O_2$ linelist

									Calculation		Observation	
V_U	V_L	Nb	Band center	S_{Min}	S_{Max}	Band Int	Int_{Min}	Int_{Max}	N_{Max}	K_a range	N_{Max}	K_a range
001	000	5860	1582.10	1500.73	1660.45	2.039E-19	2.00E-26	4.56E-22	77	0-15	70	0-13
120	000	157	2761.21	2819.67	2889.29	0.162E-22	0.21E-25	0.21E-24	42	5-5	0	0
101	000	3640	2858.71	2784.88	2890.81	1.036E-20	3.64E-28	2.34E-23	61	0-15	54	0-10

Total : 118249 lines

Caption :
V_U V_L : (v_1,v_2,v_3) vibrational assignments

Nb : number of lines
Band center: approximate band center (in cm^{-1})
SMin Smax= Wavenumber range (in cm^{-1})
Band int, Int_{Min}, Int_{Max}: band intensity, minimum and maximum value of the line strength (in $cm^{-1}/(molecule.cm^{-2})$ at 296K.
Calculation: N_{Max}:, K_a range: maximum value of N, minimum and maximum value of K_a for the upper state in the calculated linelist
Observation: N_{Max}:, K_a range: maximum value of N, minimum and maximum value of K_a for the upper and lower experimental energy levels used for the computation.

Table 4

(see the separate file)
Description of the GEISA-19database

Table 5

		Obs	$	TW			HIT		
N K_a K_c J - N K_a K_c J	vib			Sigma	E_L	E_U	Sigma	E_L	E_U
42 0 42 + 41 1 41 +	110 000	2090.6336(2)	G	2090.6330	722.2130	2812.8460	2090.6366	722.2130	2812.8496
42 0 42 - 41 1 41 -	110 000	2090.6336(2)	G	2090.6345	722.3139	2812.9484	2090.6353	722.3139	2812.9492
42 0 42 + 41 1 41 +	110 010			1341.8081	1471.0379	2812.8460	1341.8173	1471.0399	2812.8572
42 0 42 - 41 1 41 -	110 010			1341.8076	1471.1408	2812.9484	1341.8134	1471.1389	2812.9523
33 1 33 + 32 0 32 +	110 000	2090.6234(2)	G	2090.6234	443.0513	2533.6747	2090.6230	443.0513	2533.6743
33 1 33 - 32 0 32 -	110 000	2090.6408(2)	G	2090.6410	443.1170	2533.7580	2090.6380	443.1170	2533.7550
33 1 33 + 32 0 32 +	110 010			1341.5283	1192.1464	2533.6747	1341.5309	1192.1609	2533.6918
33 1 33 - 32 0 32 -	110 010			1341.5444	1192.2136	2533.7580	1341.5438	1192.2109	2533.7547
35 8 27 + 36 8 28 +	011 010	1557.1093(2)	G	1557.1085	1808.5312	3365.6397	1557.1130	1808.5329	3365.6459
35 8 27 - 36 8 28 -	011 010	1557.1093(2)	G	1557.1095	1808.2940	3365.4035	1557.1150	1808.2999	3365.4149
35 8 27 + 36 8 28 +	011 000		G	2327.4023	1038.2374	3365.6396	2327.4101	1038.2374	3365.6475
35 8 27 - 36 8 28 -	011 000		G	2327.3855	1038.0178	3365.4033	2327.3941	1038.0178	3365.4119
45 4 41 + 46 4 42 +	011 010	1557.4479(2)	G	1557.4488	1787.5838	3345.0326	1557.4630	1787.5839	3345.0469
45 4 41 - 46 4 42 -	011 010	1557.4479(2)	G	1557.4476	1787.5899	3345.0375	1557.4610	1787.5729	3345.0339
45 4 41 + 46 4 42 +	011 000		G	2311.9175	1033.1151	3345.0326	2311.9282	1033.1151	3345.0433
45 4 41 - 46 4 42 -	011 000		G	2311.9143	1033.1233	3345.0376	2311.9252	1033.1233	3345.0485
27 10 17 + 28 10 18 +	011 010	1557.4704(2)	G	1557.4698	1858.4606	3415.9304	1557.3910	1858.1159	3415.5029
27 10 17 - 28 10 18 -	011 010	1557.4704(2)	G	1557.4698	1857.9318	3415.4017	1557.3870	1858.6289	3416.0199
27 10 17 + 28 10 18 +	011 000		G	2337.9880	1077.9428	3415.9309	2338.1092	1077.4496	3415.5588
27 10 17 - 28 10 18 -	011 000		G	2337.9523	1077.4496	3415.4019	2338.1409	1077.9428	3416.0837
31 9 22 + 32 9 23 +	011 010	1557.5094(2)	G	1557.5097	1820.1611	3377.6708	1557.4900	1820.2009	3377.6909
31 9 22 - 32 9 23 -	011 010	1557.5094(2)	G	1557.5107	1819.7996	3377.3103	1557.4910	1819.8479	3377.3389
31 9 22 + 32 9 23 +	011 000		G	2332.7906	1044.8802	3377.6708	2332.8372	1044.8802	3377.7174
31 9 22 - 32 9 23 -	011 000		G	2332.7661	1044.5441	3377.3102	2332.8146	1044.5440	3377.3586

21 3 19 + 20 2 18 +	020 010	809.0824(1)	G	809.0826	958.7949	*1767.8775*	809.0826	958.7949	*1767.8775*
21 3 19- 20 2 18 -	020 010	809.0445(1)	G	809.0438	958.7871	*1767.8309*	809.0438	958.7871	*1767.8309*
21 3 19 + 20 2 18 +	020 000		G	1560.0222	207.8553	*1767.8775*	1560.0103	207.8553	*1767.8656*
21 3 19- 20 2 18 -	020 000		G	1559.9817	207.8493	*1767.8310*	1559.9695	207.8493	*1767.8188*
20 3 18 + 21 3 19 +	021 020	1572.9332(2)	G	1572.9346	*1767.8774*	3340.8120	1572.9378	*1767.8793*	3340.8171
20 3 18 - 21 3 19 -	021 020	1572.9332(2)	G	1572.9322	*1767.8310*	3340.7632	1572.9359	*1767.8313*	3340.7672
20 3 18 + 21 3 19 +	021 010			2324.9823	**1015.8297**	3340.8120	2324.9839	**1015.8349**	3340.8188
20 3 18 - 21 3 19 -	021 010			2324.9750	**1015.7882**	3340.7632	2324.9771	**1015.7949**	3340.7720
20 3 18 + 21 3 19 +	021 000	3077.7153(3)	G	3077.7153	263.0968	3340.8121	3077.7192	263.0968	3340.8160
20 3 18 - 21 3 19 -	021 000	3077.7036(3)	G	3077.7033	263.0598	3340.7631	3077.7078	263.0598	3340.7676
23 0 23 + 24 0 24 +	201 200		G	1530.9994	2876.7510	4407.7504	1531.0200	2876.7552	4407.7752
23 0 23 - 24 0 24 -	201 200		G	1531.0282	2876.7998	4407.8279	1531.0171	2876.7993	4407.8164
23 0 23 + 24 0 24 +	201 000	4155.4091(2)	G	4155.4106	252.3398	4407.7504	4155.4340	252.3398	4407.7738
23 0 23 - 24 0 24 -	201 000	4155.4467(2)	G	4155.4439	252.3841	4407.8280	4155.4439	252.3841	4407.8280

Caption :
N K_a K_c J - N K_a K_c J: Rotational assignments
Vib: vibrational transition
Obs: (when possible) Observed line positions: (1) Line assigned in Ref. [29]; (2) on spectrum FTS3, FTS12, , or FTS113 (see Fig. 1, Fig. 4, Fig. A3 or Fig. A7 for example). (3) Lines assigned in Ref. [34].
TW: This work.
$: a "G" indicates the lines which are quoted in GEISA-19.
HIT: HITEMP database.

This work: results of the present work. G-19 if included in GEISA-19.
E_U and E_L: upper and lower state energy level

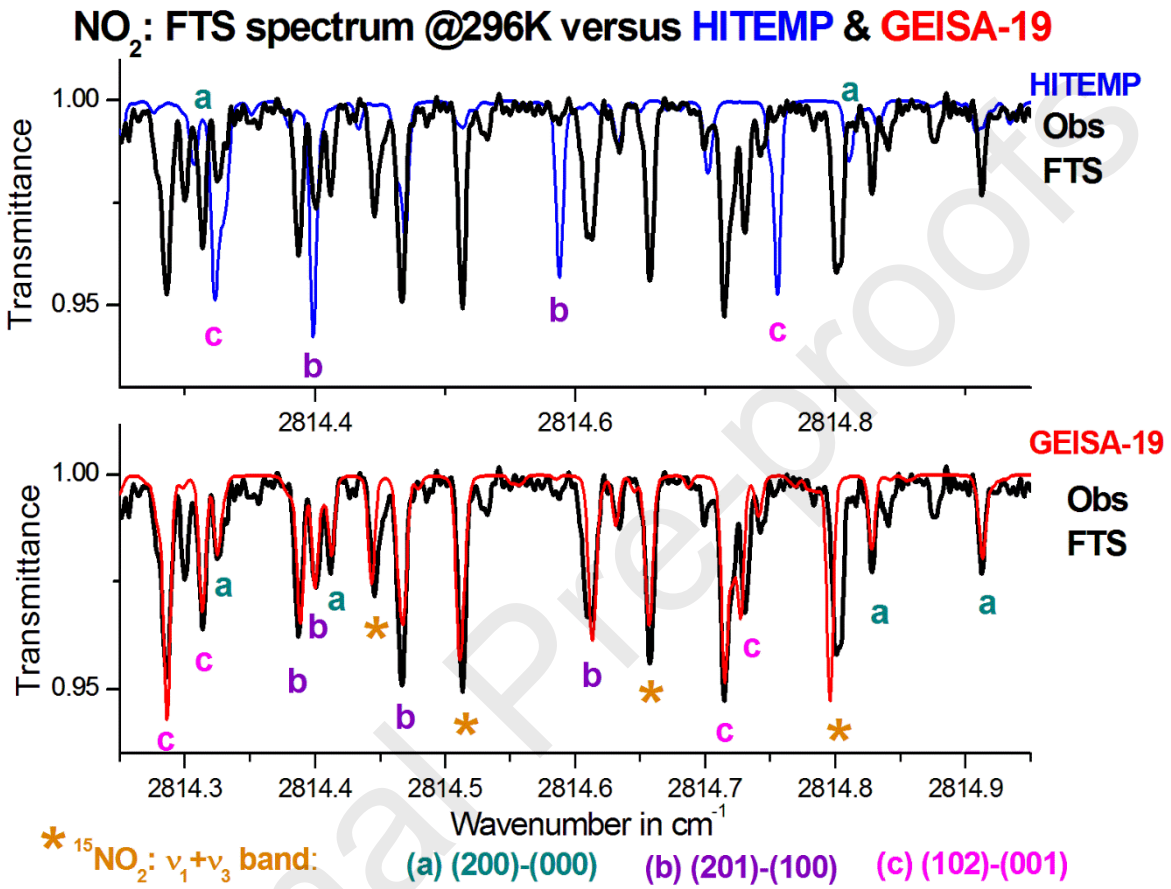

Highlights

New lists of line position, line intensity and line shape parameters of nitrogen dioxide (GEISA-19) for GEISA (https://geisa.aeris-data.fr/).dioxide. $^{14}N^{16}O_2$ and $^{15}N^{16}O_2$. 1153-4775 cm^{-1}. Validation with high resolution Fourier transform spectra. Inter-comparison with HITEMP and HITRAN2016-updated. First identification of the $\nu_1+2\nu_3-\nu_3$ hot band.

First determination of the (1,0,2) energy level parameters and an improved set of parameters for the (0,1,1) vibrational state.